PL-TR-96-3035

Diagnostics Development of Plasma Thrusters: Comprehensive Investigation of Low-Power Arcjet Operation

Daniel Erwin

Department of Aerospace Engineering
University of Southern California
University Park
Los Angeles CA 90089-1191

September 1998

Final Report

APPROVED FOR PUBLIC RELEASE; DISTRIBUTION UNLIMITED.

AIR FORCE RESEARCH LABORATORY
AIR FORCE MATERIEL COMMAND
EDWARDS AIR FORCE BASE CA 93524-7048

NOTICE

When U.S. Government drawings, specifications, or other data are used for any purpose other than a definitely related Government procurement operation, the fact that the Government may have formulated, furnished, or in any way supplied the said drawings, specifications, or other data, is not to be regarded by implication or otherwise, or in any way licensing the holder or any other person or corporation, or conveying any rights or permission to manufacture, use or sell any patented invention that may be related thereto.

FOREWORD

This final technical report presents the results of a study performed by the Department of Aerospace Engineering, University of Southern California, Los Angeles, CA, under Contract No. F04611-92-K-0004 for the Air Force Research Laboratory (AFRL), Propulsion Directorate, Edwards Site (formerly OL-AC Phillips Laboratory), Edwards AFB CA 93524-7048. The project manager at AFRL was Dr. Ronald Spores.

This report has been reviewed and is approved for release and distribution in accordance with the distribution statement on the cover and on the SF Form 298.

Ronald Spores

RONALD A. SPORES
Chief
Spacecraft Propulsion Branch

Jeff Vesselenk for

RANNEY G. ADAMS III
Public Affairs Director

Lawrence P. Quinn

LAWRENCE P. QUINN
Technical Advisor
Propulsion Engineering Division

REPORT DOCUMENTATION PAGE

Form Approved
OMB No 0704-0188

1. AGENCY USE ONLY (LEAVE BLANK)	2. REPORT DATE	3. REPORT TYPE AND DATES COVERED
	September 1998	Final Report, 31 Dec 91-30 Jun 94

4. TITLE AND SUBTITLE
Diagnostics Development of Plasma Thrusters: Comprehensive Investigation of Low-Power Arcjet Operation

5. FUNDING NUMBERS
C: F04611-92-K-0004
PE: 62302F
PR: 3058
TA: 00DX

6. AUTHOR(S)
Daniel Erwin

7. PERFORMING ORGANIZATION NAME(S) AND ADDRESS(ES)
Department of Aerospace Engineering
University of Southern California
University Park
Los Angeles CA 90089-1191

8. PERFORMING ORGANIZATION REPORT NUMBER

9. SPONSORING/MONITORING AGENCY NAME(S) AND ADDRESS(ES)
Air Force Research Laboratory (AFMC)
AFRL/PRRS
4 Draco Drive
Edwards AFB CA 93524-7190

10. SPONSORING/MONITORING AGENCY REPORT NUMBER
PL-TR-96-3035

11. SUPPLEMENTARY NOTES Air Force Research Laboratory was formerly OL-AC Phillips Laboratory.
COSATI CODE(S):

12a. DISTRIBUTION/AVAILABILITY STATEMENT
Approved for public release; distribution is unlimited

12b. DISTRIBUTION CODE
A

13. ABSTRACT (MAXIMUM 200 WORDS)

Two experimental diagnostic techniques were developed and applied to plume measurements of low-power (1-kW class) hydrogen arcjets. The outstanding experimental problem of measurement of plume species density was addressed using two-photon, laser-induced fluorescence. Current-modulation velocimetry was applied to the study of plume velocity fluctuations and it was found that they exhibited no correlation with the supply current ripple and appeared to be random.

14. SUBJECT TERMS
plasma technology; electric propulsion; space propulsion

15. NUMBER OF PAGES
42

16. PRICE CODE

17. SECURITY CLASSIFICATION OF REPORT	18. SECURITY CLASSIFICATION OF THIS PAGE	19. SECURITY CLASSIFICATION OF ABSTRACT	20. LIMITATION OF ABSTRACT
Unclassified	**Unclassified**	**Unclassified**	**SAR**

NSN 7540-010280-5500

Standard Form 298
(Rev 2-89)
Prescribed by ANSI Std 239-18
298-102

TABLE OF CONTENTS

LIST OF FIGURES

GLOSSARY

ASE	amplified spontaneous emission
CMV	current-modulation velocimetry
LIF	laser-induced fluorescence
LoS	line of sight
MPI	multiphoton ionization
PMT	photomultiplier tube
PPU	power-processing unit
RC	resistance-capacitance

1.0 INTRODUCTION

Arcjets are expected to play an increasing role in satellite propulsion needs, primarily for stationkeeping and on-orbit maneuvering in the near term. While the technology is considered viable enough to be deployed on a Telstar IV communications satellite for stationkeeping,[1] arcjet technology is far from maturity. To compete successfully with chemical propulsion systems for on-orbit missions, further improvements in arcjet propulsion systems are still required.[2] If needed improvements in the performance level and efficiency of arcjets are to be achieved, an increased understanding of the fundamental physical processes that govern the operation of an arcjet is essential. In addition, the ability to predict the plume behavior of a space propulsion device is necessary for prediction and amelioration of damaging plume-spacecraft interactions.

Significant arcjet energy loss results from velocity profile losses due to thick internal boundary layers in the arcjet nozzle and from frozen flow losses such as molecular dissociation. To quantify profile losses, both gas velocity and density distributions must be known. In addition, arcjet models, which are necessary for timely and cost-effective design improvements, must be tested by comparing them to key physical parameters.

For measuring excited-state atomic hydrogen velocity and temperature, excited-state laser-induced fluorescence[3,4] has proven to be accurate and essentially nonintrusive. Though the excited states of hydrogen are more easily accessible, most atoms in the plume region are expected to be in the ground state. The ability to measure ground-state atomic hydrogen temperature and velocity in addition to density would allow examination of any differences in temperature and velocity between the excited-state and ground-state species in the nonequilibrium arcjet plume environment. Moreover, computational calculation of thruster efficiency is based on momentum flux, so that exhaust density as well as velocity must be known.

At present, only limited inroads have been made into the problem of plume density measurements. For hydrogen arcjet thrusters, determination of species density has previously only been accomplished through the use of absorption spectroscopy techniques.[5,6] These vacuum- and extreme-ultraviolet spectroscopy approaches are quite difficult to implement in practice and are limited to determination of line-of-sight averaged number densities at downstream locations in the plume where the optical depth is not high. These techniques have not been applicable in the determination of atomic density profiles at the thruster nozzle exit, data that are desired in order to calibrate and verify recent advanced computational arcjet modeling results.[7–12]

The density of atoms relative to the density of molecules in the arcjet thruster is an indication of how much energy is lost into dissociation of the hydrogen molecules and not recovered through recombination into translational kinetic modes. To determine the molecular dissociation fraction and the significance of this energy loss mechanism, the molecular species density, as well as the atomic number density, need to be known. The recent use of Raman spectroscopy[13,14] in an arcjet plume has provided the first information on molecular hydrogen densities at the arcjet nozzle plane.

It has become obvious that there is a need for determination of atomic ground-state hydrogen densities at the nozzle exit of the hydrogen arcjet to support ongoing modeling efforts and to quantify the significance of frozen flow losses such as molecular dissociation.

In this work, the approach taken for density measurement is two-photon laser-induced fluorescence.

Several of the computational approaches to arcjet simulation are, in principle, time-accurate. Therefore, they may be used to investigate instability or fluctuations in arcjet operation (arc length fluctuation, rotation of anode attachment spot, etc.). These time-dependent phenomena may be inherent to arcjet operation or may be caused by interaction with the power-processing unit. However, experimental diagnostic techniques such as laser-induced fluorescence perform time-averaging and, thus, give results averaged over any fluctuations.

To address this, a time-resolved technique, current-modulation velocimetry, which has demonstrated significant fluctuations in arcjet plume velocity, was developed under this contract.

2.0 WORK PERFORMED

2.1 Two-Photon Laser-Induced Fluorescence

2.1.1 Introduction. Recent advances in flame diagnostics indicate that methods used for observing concentrations of atomic hydrogen in flames using two-photon or multiphoton laser-induced fluorescence (LIF) may be applicable to arcjet plumes. This part of the work consists of examination of these techniques and their application to the measurement of ground-state hydrogen atom concentrations.

Observing atomic hydrogen during its lifetime in a nonintrusive manner often involves optical detection of the emission from radiating excited electronic states or the measurement of photon absorption through a population of atomic hydrogen. Inducing the fluorescence with laser light tuned to a specific transition frequency, i.e., LIF, can allow information on the species participating in the electronic transition to be inferred. Usually, the excited states of hydrogen are probed as the excited-state transitions are more accessible to laser equipment currently available and can be detected in the visible wavelength range.

In a nonequilibrium plasma such as the arcjet plume, the excited-state population of atomic hydrogen cannot be used to infer the ground-state hydrogen population. Therefore, it is necessary to identify a direct method of probing the ground state of hydrogen.

In the flame environment, atomic hydrogen plays an important role in the chemistry of most combustion processes. Measuring ground-state hydrogen profiles in premixed flames is considered critically important in understanding how to best model the combustion processes of flame chemistry. The development of laser diagnostics to non-intrusively probe ground-state

hydrogen atoms has been explored in depth during the last decade to facilitate these measurements.

Research in this field has centered on three excitation schemes of ground-state hydrogen: two-photon direct excitation, three-photon direct excitation, and two-step, three-photon excitation. The last scheme was developed at Sandia National Laboratory; work on the other two schemes has also been examined in detail at Sandia as well as at numerous other institutions. An overview of these schemes is given in the following sections.

Researchers at Sandia[15–23] examined the uses of multiple-photon stimulated emission to promote ground-state radicals to an excited state whereby emission in the visual wavelength region could be detected. Problems inherent in the technique were investigated and included the dependence of the emission signal on three parameters: laser power, ambient gas pressure, and the spectral shape of the stimulated emission. Multiple-photon excitation schemes were found to have increased sensitivity to each of these parameters compared with standard single-photon laser-induced fluorescence.

This diagnostic approach to the hydrogen atom was demonstrated using a two-step method where a two-photon transition was used to excite the ground state of hydrogen to the first excited state (n=2) and then a resonant detection scheme, requiring a second laser, excited some of those placed in the first excited state to the second excited level (n=3) via a single-photon transition. The resulting decay from n=3 to n=2 was observed.

The n=1 to n=2 transition requires a single photon at a wavelength of 121.5 nm or a two-photon transition at 243 nm (the absorption cross-section for a two-photon transition is substantially smaller than for a single-photon transition and will be discussed later in Section 2.1.2). The latter wavelength is more desirable for two reasons. The 243-nm light is much more easily created with the laser technology available today (including doubling/tripling crystals and pressure cells) and wavelengths below 200 nm are easily absorbed by the atmosphere and require a vacuum path for the entire path of the beam.

To complete the two-step method, an additional 656-nm beam promoted those atoms that were previously excited (based on the cross-section probability) to n=3. Subsequent detection of 656-nm emission was observed.

Comparison of this technique with direct two-photon and three-photon schemes was conducted by researchers at Sandia[22] and found to provide more accurate results for rich hydrocarbon flames, though the results for most simple flames were identical. The two-step technique may be more difficult to implement than the other techniques since it requires two lasers (though a variation using different transitions can be accomplished with only one laser), making the experiment more complex and costly.

One of the side effects of the multiphoton direct excitation techniques in hydrogen is that they directly promote ground-state electrons to the second excited level, causing a potential population inversion between the first excited state and the second excited state. This takes place only along

the line of irradiation by the ultraviolet laser beam (typical for irradiation of ground-state hydrogen atoms) and can lead to the creation of an additional laser beam (in the visible for hydrogen when, for example, Hα radiation is initiated) along the path of the initial beam. This reabsorption of emitted photons can cause a problem if a measurement is attempting to create an analog between light collected and the density of emitters and must either be accounted for or avoided.

Researchers at Sandia were the first to examine this optically excited stimulated emission (sometimes called amplified spontaneous emission or ASE) and its relationship to the multiphoton fluorescence diagnostic. One of the important observations was that while the fluorescence due to the excitation followed a laser power-squared behavior, the ASE fluorescence went as laser energy to a higher exponential power, so that it could dominate at higher laser energies and drop to an insignificant process at lower laser energies.

The use of ASE itself as a diagnostic was examined, but its line-of-sight nature and the requirement of transition saturation before a linear relation between species density and signal is observed led to difficulties in application.

To use the multiphoton diagnostic technique as a measure of atomic hydrogen density, a correlation between the number of emitters and the measured fluorescence is required. A process that can prematurely depopulate atoms excited by the diagnostic is collisional quenching due to even a moderately high-pressure environment. Sandia looked at the time-resolved fluorescence decay of the atomic hydrogen in low pressure flames (20 mtorr) to examine the relationship of pressure to quenching for this diagnostic technique and characterized the relationship between the fluorescence decay times and the expected attenuation of the emitted fluorescence. Changes in pressure, and correspondingly in quenching, can be determined through observation of changes in fluorescence decay times of the LIF.

Relative hydrogen density measurements were compared with flame models using these techniques and the results were found to agree well. However, it was not known if calibrated atomic hydrogen density measurements were made at Sandia.

At the University of Stuttgart,[24–27] detailed examinations of quenching, excitation linewidth, and fluorescence calibration for two-photon LIF diagnostics on atomic hydrogen in flames have been performed. Direct two-photon LIF at 205 nm was implemented to promote ground-state hydrogen atoms to the n=3 excited state where n=3 to n=2 (Hα) fluorescence was observed. Key to the work performed at Stuttgart was detailed calibration of the fluorescence using a calibration cell containing atomic hydrogen created from a microwave discharge. Hydrogen densities in the cell were determined using a chemical gas titration technique, discussed in Section 2.1.3.

This technique was successfully demonstrated near a heated filament where pressures ranged from 1 to 100 mbar (100 to 10,000 Pa) and the hydrogen source came from a 5% CH_4 chamber environment. Quenching effects were calculated in pressure ranges above 10 mbar and determined from fluorescence lifetime decay rates at lower pressures as described earlier in this section.

Researchers at Ohio State University[28,29] have also done several similar multiphoton LIF experiments. Of interest in this work is additional attention to detail involving chemical titration calibration of two-photon LIF and corrections for collisional quenching. Atomic hydrogen density is determined in a calibration cell using titration of small amounts of NO_2 to chemically react with hydrogen atoms present in the cell. Additionally, the fine structure of the n=3 state of atomic hydrogen was examined in order to determine the unquenched radiative lifetime of this excited state when populated by a two-photon excitation process. This lifetime is important in determining the correction factor applied to a quenched signal through measurement of fluorescence decay.

Kyushu University[30,31] closely compared four different two-photon excitation schemes. They found that unless hydrogen densities are very low ($<10^{11}$ cm^{-3}), losses in detecting vacuum ultraviolet emission require the use of fluorescence emission in the visible to detect hydrogen atoms, which constrains the choice of excitation level to either the n=3 or n=4 excited state. Of these options, the Kyushu group determined that two-photon excitation into the n=3 level and the subsequent observation at the Hα wavelengths produced the largest number of fluorescence photons per incident laser photon. This also was the best choice if molecular dissociation due to the incident laser was to be avoided and if incident intensities were to be kept low (to avoid ASE, for example). In addition, two-photon excitation from n=1 to n=3 also appeared to be the least sensitive to collisional quenching of the four techniques that were examined. Because of all of the above advantages, it appeared that for an environment somewhat similar to that in electric propulsion plasmas, the two-photon to n=3 scheme appeared to be the technique of choice.

2.1.2 Laser-Induced Fluorescence – General Discussion. LIF spectroscopy has gained wide acceptance in the past two decades as a diagnostic technique that generates measurable fluorescence from a small species population that otherwise might not be detectable.[32] Fluorescence, the spontaneous emission of radiation from upper energy levels, is observed when a population increase of an upper level is created through photon absorption, particle collision, or many other interactions, and then emits photons as the level relaxes to a lower population (see Fig. 1). Increasing the population of selective upper levels can be obtained by exciting specific lower levels of the species with the coherent light of fixed frequency. This excitation process (usually accomplished with laser light) can increase the population of the upper level for a set duration based on the population of the lower level. Fluorescence resulting from the increased population during pumping is often significantly larger than without the excitation pumping, providing a means of observing small species populations. This also allows investigation of the populations of the lower energy levels that are used to supply the upper levels.

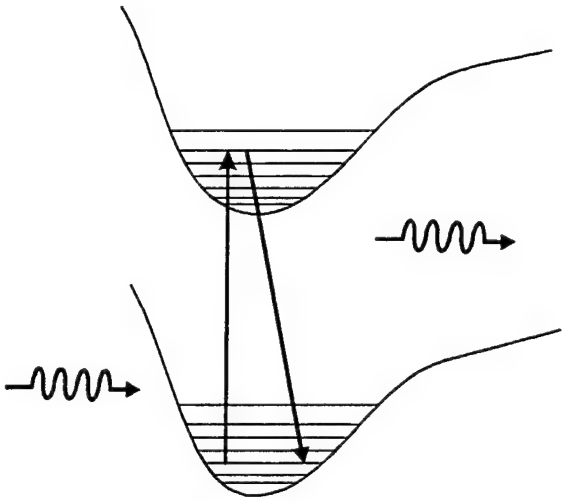

Figure 1
Absorption and Emission of Photons in LIF

Laser light used for the excitation process must be of the specific frequency that corresponds to the energy difference between the lower and upper levels of the transition being probed. To create laser light at the specific frequency required for many different transitions, tunable dye lasers are often employed to allow probing in the range from 200 nm to 1.5 mm. Probing in regions around and below 200 nm is often difficult due to atmospheric absorption, but can be avoided through the use of multiphoton processes.

Multiple photons of a frequency related to a transition spacing by an integer multiplication can induce the transition to take place. A weaker excitation cross-section is typical for multiphoton transitions when compared to the cross-section for the transition with single photons.

To perform LIF on a particular species, several criteria must be met. To properly account for the fluorescence detected from the excitation, the molecule or atom in question must have a known emission spectrum. Processes such as dissociation from the excited state can affect the fluorescence that is measured and sometimes even prevent it from being detected at all. This is also important if the fluorescence produced from exciting the species is to be related to the intensity of the pumping or the density of the species in the lower levels.

Methods for creating the light needed to pump the transition must also be available. Tunable coherent light sources are desired for use in LIF because of the need to match frequencies to atomic and molecular transitions and scan across the transition frequencies to learn information about fine structure, intensity, linewidth, etc. In different spectral ranges, different tuning methods have been developed to initiate the desired light. Devices spanning these ranges include semiconductor diode lasers, tunable gas lasers, pumped dye lasers (both pulsed and continuous-wave), and excimer lasers.[33]

The radiative decay rate from the upper excited state must be known, since the fluorescence power is proportional to that rate.[32] Moreover, as other species are present, a decrease in

excited-state population may occur due to factors other than spontaneous emission such as collisions and laser-induced chemistry. To determine species number density from the measured fluorescence, these quenching processes must be taken into account.

In the simplified case (Fig. 2) of a two-level energy system with a lower level (n=1) and an upper level (n=2), the rates for the optical and collisional processes connecting the two levels can be described by four processes and their rate coefficients: stimulated absorption (b_{12}), stimulated emission (b_{21}), spontaneous emission (A), and quenching (Q). The Einstein A and B coefficients are related to these rates in the following manner. The spontaneous emission is given by the A coefficient and the stimulated rates are related to the B coefficient through the following expression (degeneracies of the levels are ignored):

$$b_{12} = b_{21} = \frac{BI_\nu}{c} \tag{1}$$

where I_ν is the spectral irradiance, defined as the incoming laser intensity per unit frequency interval, and c is the speed of light. The stimulated rates thus depend on the incident laser intensity, linewidth, and pulse duration, as well as on the specific transition.

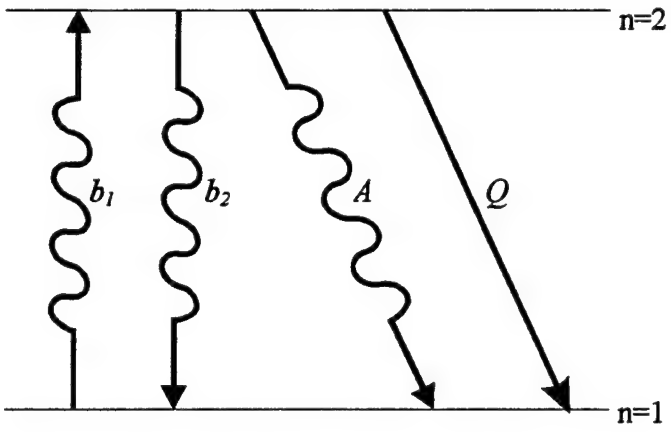

Figure 2
Two-Level Energy Diagram Showing Excitation and Relaxation Processes

The rate equations for the change in population of the two states can be written utilizing these four parameters and the populations N_1 and N_2 of the respective levels:

$$\frac{dN_1}{dt} = -N_1 b_{12} + N_2 (b_{21} + A + Q) \tag{2}$$

and

$$\frac{dN_2}{dt} = +N_1 b_{12} - N_2 (b_{21} + A + Q). \tag{3}$$

where Equations (2) and (3) allow the determination of each level's population. For the closed-system case examined, the population rate equations could be coupled assuming population conservation. By substituting for N_1 and then integrating, a relation for the upper-state population based on an exponential term in time results,[32] given by

$$N_2 = \frac{b_{12}N_T}{b_{12}+b_{21}+A+Q}\left(1-e^{-(b_{12}+b_{21}+A+Q)t}\right) \tag{4}$$

where $N_T = N_1 + N_2$ is the total population and is equal to the sum of the initial populations, and t is time. As the steady state is approached, i.e., as the exponential term approaches zero, the population of the upper level approaches the constant value

$$N_2 = \frac{b_{12}N_T}{b_{12}+b_{21}+A+Q}. \tag{5}$$

This can be rearranged, using Equation (1), to

$$N_2 = N_T\left(\frac{b_{12}}{b_{12}+b_{21}}\right)\frac{1}{1+\dfrac{A+Q}{b_{12}+b_{21}}} = \frac{N_T}{2\left(1+\dfrac{I_\nu^{sat}}{I_\nu}\right)} \tag{6}$$

where the saturation spectral intensity, I_ν^{sat}, is defined by

$$I_\nu^{sat} = c\frac{A+Q}{2B} \tag{7}$$

Thus, for the closed system case, after a time greater than the exponential characteristic time, the upper level population can be described by the ratio of spectral intensity to its saturation value.

Another approach for a more realistic system is to assume a steady state in the population of two levels and solve for the population by setting the two rates equal to zero. However, a steady state may not be achieved when laser pulses are short and laser intensities are small such that quenching processes dominate.

The observed fluorescence, F, is given by the population of the upper level, the spontaneous emission rate, the frequency of the emitted photon, and the physical irradiation volume of the laser light:

$$F = h\nu N_2 A\frac{\Omega}{4\pi}V \tag{8}$$

where $h\nu$ is the photon energy, Ω is the collection solid angle, and V is the volume comprised of the focal area of the laser beam and the length over which the fluorescence is observed. For a given optical setup probing a given transition of a particular species, the fluorescence varies only with N_2.

Transitions of interest are often found where excitation would require photons with a wavelength below 200 nm. Not only is excitation of these transitions difficult due to the absence of tunable wavelength lasers available in this range, but it is also difficult to implement because of the strong absorption at these wavelengths by the air in the laboratory and by other gases that may be present inside a test facility. Consequently, when transitions below 200 nm are intended to be pumped, a multiphoton approach (usually two or three photons) is used. Two-photon cross-sections are quite small. However, photons with half the frequency or double the wavelength can be much easier to create in the laboratory. Stimulated emission of an atom that has been excited by the two-photon process can be neglected, since it is collinear with the exciting radiation. For a two-photon process, Equation (3) becomes

$$\frac{dN_2}{dt} = +N_1 W_{12} - N_2 (A + Q) \tag{9}$$

where W_{12} is the two-photon cross-section.

Two-photon cross-sections have been measured and reported in literature[32] and cannot be directly related to single-photon cross-sections because of their representation of different processes and different units. As a rough rule of thumb, under common conditions an order of magnitude more laser intensity is required for signals similar to standard LIF when using a two-photon scheme on atomic species in an atmospheric flame.

Fluorescence due to a two-photon absorption is quadratically related to laser power, while the excited-state population is affected by quenching linearly as in single-photon fluorescence.

The specific problem of excitation of the ground state of hydrogen to its excited states requires a single photon below 200 nm or a two-photon excitation using wavelengths that are greater. Since this excitation is intended for use as a diagnostic technique, detection will be important so excitation to the second excited state (n=3) or third excited state (n=4) will be desired as relaxation to the first excited state from either of these states can be detected in the visible wavelength range (656 nm for n=3 $\rightarrow$ n=2, 486 nm for n=4 $\rightarrow$ n=2) . Excitation to the second excited state of hydrogen and the resulting fluorescence is shown in Figure 3.

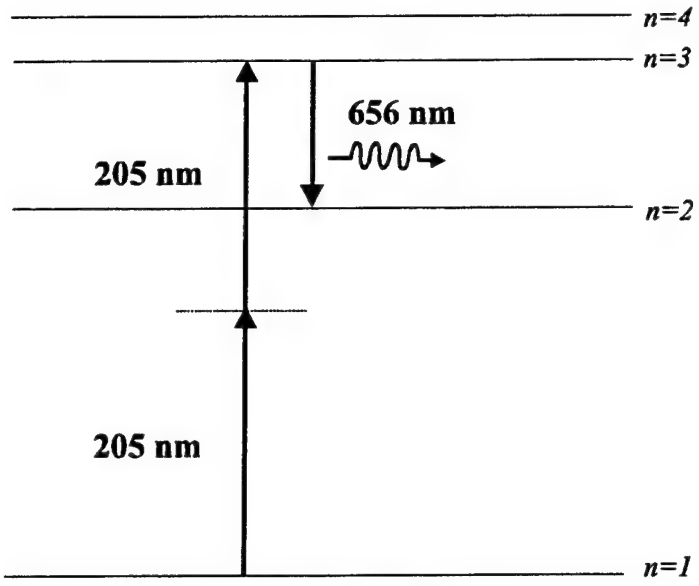

Figure 3
Two-Photon Excitation of the Ground-State Hydrogen Atom to *n*=3 and the Resulting Fluorescence
(Figure not drawn to scale)

One-photon excitation to the second excited state requires 102.5-nm photons, while a two-photon transition requires a wavelength of 205 nm, much more easily created in the laboratory through doubling or tripling of 410-nm or 615-nm laser light, which is readily available using tunable dye lasers.

One of the problems of the scheme of Figure 3 is the population inversion created between the first and second excited states when directly pumping ground-state atoms to the second excited state. This inversion serves as a gain medium for the 2–3 transition along the path of laser stimulation. The resulting ASE complicates the interpretation of the fluorescent signal and can actually create a new laser beam in the hydrogen being probed along the path of the 205-nm two-photon excitation beam.[20]

Two methods of exciting the ground state of atomic hydrogen involving three-photon excitation have been reported.[22] One involves populating the first excited state with two photons and then populating the second or third excited state with a photon of another wavelength, thus avoiding the population inversion problem and ASE. Another three-photon method involves directly populating the second excited state with three photons of the same wavelength.

Two-step LIF on ground-state hydrogen atoms uses two 243-nm photons to promote ground-state atoms to the first excited state, while a second photon at either 486 nm or 656 nm excites the atom in the first excited state to the third or second excited state, respectively. This is shown in Figure 4.

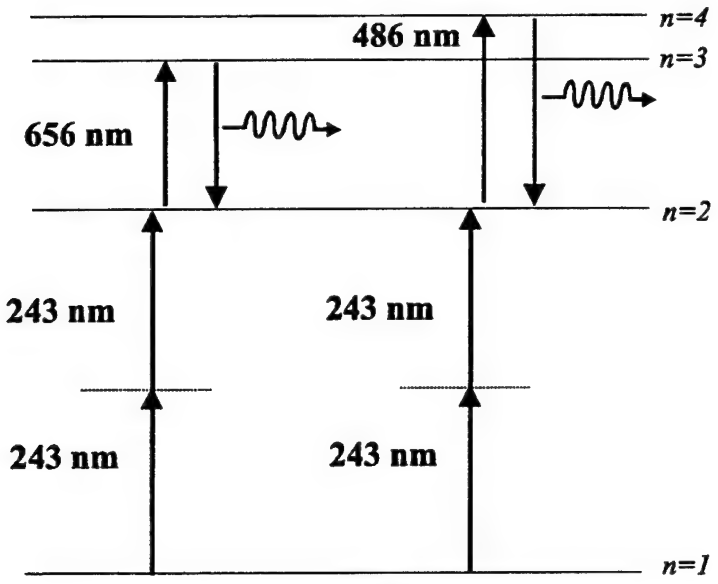

Figure 4
Two-Step, Three-Photon Excitation Schemes
(Figure not drawn to scale)

These techniques are more difficult in two respects. First, two-step excitation requires resonant detection. In other words, the light being detected is at the same wavelength as one of the laser beams and cannot be spectrally separated. The fluorescence is only separated temporally from the laser beam on a timescale related to the Einstein coefficients of the depopulation of the chosen excited state. Scattered laser light can interfere with measurement of the fluorescence signal, especially in low-signal situations, and make detection extremely difficult. Second, both techniques require a second photon to continue the excitation process once the first excited state is populated. This requires the two lasers to overlap the detection area, both spatially and temporally, for the full excitation to occur.

In the case where the second step is accomplished by a 656-nm photon, a second laser is required. If a 486-nm beam is used, one laser can produce 486 nm and some part of the beam can be doubled for 243 nm. This requires only one laser, though it must have enough energy per pulse to support each of the transitions in the environment being probed. This method is called single-laser two-step excitation and is the preferred implementation of the two-step techniques.

Two-step techniques avoid population inversions associated with other two- and three-photon excitation schemes, but add an additional layer of difficulty in both implementation and understanding of what is being probed. Instead of exciting the ground state directly to a level where fluorescence takes place, two-step excitation excites atoms to an intermediate level where they are then excited again at some rate to a higher excited state. If density measurements are to be made using this technique, a method for understanding the total cross-section of the excitation must be developed. Promotion to the final excited level occurs according to the convolution of the two laser lineshapes. This becomes even more difficult if the gas being probed is moving at high velocities (~km/s) with respect to the incoming photons, so that Doppler shifts are

significant, as in the arcjet plume environment. The first beam will excite atoms according to their relative velocity as well as density, while the second beam will also excite some part of those by velocity from a group that has already been selected by velocity. Tying the laser scan rates together by wavelength (or using one laser for both beams) may allow this problem to be overcome.

The other scheme found in the literature involves using three photons to probe ground-state hydrogen atoms.[22] Three photons at 292 nm together excite the ground state to n=4 where n=4 to n=2 fluorescence is observed. This method has not been deemed very practical because of the smaller cross-section for three-photon excitation than for two-photon excitation; moreover, it does not deal with the ASE issue any better than two-photon excitation to n=3. Additionally, when compared to the other excitation schemes, it is found to have lower signal-to-noise than the others. It does have the benefit of using the highest wavelength photons, which are more easily created in the laboratory.

2.1.3 Detecting Hydrogen Atoms in an Arcjet Plume. Of the techniques described so far, the two that appear to be of most interest are two-photon direct excitation of the second excited state and single-laser two-step, three-photon excitation to the third excited state. These techniques have been shown to adequately probe the flame environment for ground-state atomic hydrogen. They appear to be the best candidates to measure absolute density of hydrogen in an arcjet plume. The work described here employs the two-photon direct excitation method. Future work may shift to the other technique, should ASE and other properties unique to this method prove to be insurmountable.

These diagnostics can also determine velocity and temperature of the ground state of hydrogen in the arcjet plume using nearly the same experimental setup as for density measurements.

This point-specific diagnostic technique requires that at minimum, accurate spatial alignment between one laser beam and an optical detection train be maintained. Depending on the excitation technique, multiple pulsed beams are required to be aligned, not only spatially, but also temporally. Furthermore, at least one of the laser beams is in the ultraviolet spectrum and is not visible.

To satisfy this requirement, a target made of a pointed metallic rod was attached to the three-dimensional translation stage on which the arcjet is mounted. The target was set a fixed distance away from the center of the arcjet nozzle exit. For alignment of the laser beams, the rod was moved to the location observed by the detectors, while the beams were aimed onto the rod. Scattering from the tip of the rod was visible to a photomultiplier tube (PMT) with spectral filtering removed. Temporal alignment was made by observing the signal intensity on a fast oscilloscope. Differentiation between laser beams was made by blocking one or the other and observing the signal on the oscilloscope. The effect of the ultraviolet beam on the end of the metal rod could be seen as a spark with the present laser equipment, and the ultraviolet beam could be seen to fluoresce on a high-cotton-content business card (many different cards were tested and there is an amazing difference between them). After alignment, the motion-control axes were returned to their arcjet-centric home position. Absolute position within the arcjet

plume could not be made even with respect to arcjet nozzle position, so scanning through the plume in each axis was required to determine plume center and nozzle exit location.

Velocity measurements of the plume were taken with respect to the laser beam's orientation. Accordingly, two laser beam paths were used to measure axial velocity (beam shining into arcjet nozzle) and radial/azimuthal velocities (beam shining perpendicular to nozzle exit normal vector).

Because these techniques are very sensitive to laser power, strict control over laser power must be maintained. Power measurements were made regularly between scans to verify constant laser power, while pulse-to-pulse measurements during the scan were used to calibrate intensity data.

Detection of the fluorescence in the bright arcjet plume is a difficult problem and is one of the factors driving the laser power. Increased laser power increases fluorescence for a given density of atoms in the probe volume, allowing the signal to more easily be observed over the background radiation, but also leading to multiphoton ionization, ASE, and saturation, which must be avoided to accurately interpret the signal. Efficiency in signal collection is thus required.

Because the PMT is continuously exposed to the luminous plume radiation, the average current in the dynode chain is quite high. Under typical conditions, the PMT current-source circuitry is thus close to saturation. This is avoided by the use of a gated PMT socket (Hamamatsu), which is gated on only during a narrow window around the LIF events. This provides an increase of roughly an order of magnitude in effective sensitivity, since the cathode voltage can be higher than without the gated socket.

To most efficiently collect light from the arcjet plume, a lens was placed as close as possible to the arcjet nozzle exit while avoiding melting the lens or its mount. The lens collimated the collected light and a second lens focused the light onto the PMT. Bandpass interference filters were placed in front of the PMT outside the chamber. Signal from the PMT was digitized by a digital oscilloscope to determine the signal lifetime and laser pulse width, and collected by a gated integrator to amplify and average the signal from shot to shot.

Accurate understanding of the collection volume is important. The collection volume is the intersection of the laser beam cross-section with the detection focus cross-section. Determining the size of the laser beam at the point of the detection is important for this calculation and was accomplished by imaging the beam onto a photodiode near the collection volume with the laser source on the other side of the collection volume. A razor blade, attached to a motion control stepper motor system, was passed through the collection volume. By slowly moving the razor blade through the beam, the size of the beam from fully blocked to not blocked could be determined. Assuming a Gaussian laser shape, the beam waist could be determined from half the trace of intensity versus position.

A light source could be placed in the PMT housing with the tube removed to image light to the collection volume backward along the optical train. The detection focus cross-section was measured as just described, with the razor blade scanned across the illuminated collection area, but with the illumination coming from the PMT housing instead of from the laser.

To make spatial profiles of atomic density in the arcjet plume, the diagnostic had to be applied to several locations across the arcjet nozzle exit. Rather than moving the entire optical detection train and the laser optics, movement of the thruster itself on a three-dimensional motion control axis was chosen. This allowed the optics to be aligned once and remain fixed from then on. To interpret axial position data, the nozzle exit was considered to be the point where signal drops to half of its value. This assumes that the atomic hydrogen density does not drop significantly in the vicinity of the nozzle exit.

To accurately differentiate density, temperature, and velocity measurements, Gaussian profiles were least-squares fitted to spectral profiles at each spatial location in the plume where density is to be measured. (No significant differences were found among the results of using Lorentzian, Voigt or Gaussian profiles.) This allowed accurate determination of line centers, line widths, and line areas. Each measured profile was fit to a Gaussian profile using a Levenberg-Marquardt least-squares fit.[34] The shift in wavelength of the center of the line profile, with respect to the line profile of a simultaneously probed stationary gas, yielded the velocity component in the direction of the laser beam. Thus, axial velocity was measured when the laser beam was focused down the axis of the thruster into the nozzle, and the radial or azimuthal velocity was measured when the beam was directed perpendicular to the nozzle exit normal vector. The width of the Gaussian profile then yielded the temperature of the gas.

Density measurements were made based on accurate integration of the absorption lineshape of the transition probed. Fluorescence signals from different parts of the arcjet plume, as well as from a calibration environment (discussed below in this section), were related to each other for relative and absolute density measurements. This could only be successful if the integrated fluorescence in each area of the plume (and calibration cell) was understood with respect to the appropriate broadening mechanisms and artificial depopulation mechanisms taking place at different spatial locations in the plume.

One line-broadening mechanism that must be addressed is saturation broadening due to high laser energies. This mechanism could be observed (along with other mechanisms described below) when the integrated fluorescence signal deviates from the power-squared relationship between laser power and total fluorescence present.

A small amount of line broadening is caused by the linewidth of the dye laser beam which, unlike that of continuous-wave ring dye lasers, is non-negligible compared with the atomic linewidth. The laser linewidth of the available dye laser when tripled to 205 nm (for the two-photon direct technique) was measured by taking an LIF spectrum of NO gas in a calibration cell. Since NO is much heavier than hydrogen and is at room temperature instead of the much higher arcjet exhaust temperature, the width of the rotational lines in the LIF spectrum reflected only the linewidth of the laser (as long as care was taken to use unblended rotational lines). The result was that the laser had a width of 0.28 cm^{-1} (0.012 Å) at 205 nm. The effect of the laser width is taken into account using the following relation:[35]

$$\Delta\nu = \sqrt{\Delta\nu_D^2 + 2\Delta\nu_l^2} \tag{10}$$

where $\Delta\nu_D$ is the true Doppler width of the line in cm^{-1}, $\Delta\nu_l$ is the width of the laser, $\Delta\nu$ is the measured transition width, and the factor of 2 is due to the two-photon probe method.

Stark broadening mechanisms are also present in the arcjet plume and need to be understood and quantified. Stark broadening is not expected to affect the density measurements significantly and is expected to be of greatest concern for temperature measurements where the temperature is determined as related to the square of the linewidth. The effect of Stark broadening as it relates to the overprediction error in measuring temperature due to unknown electron densities is discussed in more detail later in this section.

When looking at the total convolved lineshape, the Doppler broadening component dominates and the Stark component is minimal. If the laser linewidth is deconvolved from the total linewidth before modeling, and the laser power is kept low enough to avoid saturation, a Gaussian profile with the appropriate uncertainty due to Stark effects appears to adequately model the transition linewidth.

The arcjet plume environment has substantial density gradients as the plume expands from the thruster nozzle exit. The changes in density with respect to position result in changing effects of collisional depopulation of excited-state hydrogen atoms. Correction for the quenching rate at the location of the measurement must be made.

One method of determining the quenching correction is to observe the lifetime of the fluorescence signal on a fast 500-MHz digitizing oscilloscope. The lifetime of the transition can be determined by finding the $1/e$ time of the exponential decay of the fluorescence observed. The measured signal decay is a convolution of the laser pulse decay and the transition decay and must be deconvolved prior to the measurement. Relating the lifetime at each point in the plume to the unquenched lifetime gives a linear correction factor for the measured integrated fluorescence at that point; the effective unquenched signal can then be determined in order to determine a relative density measurement. Calibration of the signal is required to convert the relative density measurement to an absolute number density. The expected density error cannot be presently obtained, since the number of contributing factors is large and the errors in many of the factors (including calibration) have yet to be determined.

A focused pulsed laser beam creates a very high instantaneous energy density, which is needed to excite the two-photon transition, but also may induce other nonlinear processes. Multiphoton ionization (MPI) will occur, and partial saturation of the transition becomes possible, even though the two-photon absorption cross-section is very small. In addition, ASE will take place for the direct two-photon excitation technique, since a population inversion is created between the pumped n=3 level and the nearly empty n=2 level. The population inversion can cause gain to occur for any photon emitted in the forward or backward direction along the laser beam.[21,36,37] If ASE or MPI become large, it results in a non-negligible loss mechanism for the LIF process. Saturation will cause power broadening of the Doppler profile of the transition and saturation, ASE or MPI will cause the power dependence of the LIF signal to deviate from the expected behavior proportional to the square of the laser power.

A preliminary laser study showed that the fluorescence signal in the arcjet plume follows power-squared behavior at low laser powers and deviates substantially from the power-squared correlation at laser powers higher than 0.05 mJ/pulse. Finding a way to detect the fluorescence in the plume accurately enough for detailed spectral profiles, while remaining at these low laser powers, will be of great importance in avoiding saturation, MPI, and ASE.

Temperature measurements are based on accurate determination of the Doppler line broadening due to thermal gas motion. Understanding the component of linewidth directly associated with Doppler broadening is essential for temperature determination. Temperature is based on the square of the measured Doppler width and can be written in terms of width in the following manner (SI units):[33]

$$\delta\lambda = 7.16\times10^{-7}\lambda_0\sqrt{\frac{T}{M}} \tag{11}$$

where $\delta\lambda$ is the linewidth due to Doppler broadening, λ_0 is the zero velocity line center, M is the molecular weight of the gas, and T is the translational temperature. Note that when solving for the temperature based on the Doppler linewidth, the width is squared and any error associated with the measurement of Doppler width is also squared. Because of this relationship, it is expected that error in measurement of temperature may be significant and could be ±30% based on preliminary findings.

One broadening mechanism that will be present and must be taken into account for accurate determination of Doppler line widths is Stark broadening of the desired atomic hydrogen transition caused by free-electron motion in the arcjet plume. In this study, a direct measurement of the profile of the electron number density for the arcjet was not made, but it was measured for nearly identical conditions[28] to be less than 2×10^{13} cm^{-3} at maximum in the center of the nozzle exit plane. This value of n_e would yield a Stark width of 0.002 Å for the Lβ line.[38] A simulated Voigt profile using this Lorentzian width shows that, for a typical measured linewidth of 0.029 Å, accounting for the Stark broadening would cause the temperature from the Doppler portion of the linewidth to go down from 1600 K to 1490 K. This represents a likely maximum Stark-broadening uncertainty in the temperature and will be greatest at the center of the nozzle where n_e is largest.

Velocity was measured by observing the Doppler shift of the absorption line and determining the velocity relative to the incoming photons responsible for the shift:

$$v = \frac{\Delta\lambda}{\lambda_0}c \tag{12}$$

where v is the velocity, $\Delta\lambda$ is the wavelength shift, λ_0 is the zero velocity line center, and c is the speed of light. The line center of each profile was determined using the Gaussian fitting process described earlier in this section. Performing the procedure simultaneously on both a static gas in a

calibration cell and in the arcjet plume provided a shifted Gaussian in the arcjet plume and a calibration of zero velocity in the calibration cell. Determination of the shift $\Delta\lambda$ between the two profiles allowed the use of Equation (12) to determine gas velocity.

In arcjet plumes, velocity of species has been seen to vary from 5 km/s to 15 km/s using the above technique with accuracy as high as 50 m/s with continuous-wavelength lasers and accuracy somewhat less resolved with pulsed lasers. In this case, resolution is a factor of 6 less than typical LIF velocity measurements that probe at 656 nm, since the transition being probed has an effective transition wavelength of 102.5 nm. Even with this constraint, velocity measurements of the ground state should still be quite accurate, with resolution expected to be about 500 m/s.

The experimental setup is shown in Figure 5. An industry-standard 1-kW arcjet thruster operating on hydrogen propellant was run in a vacuum chamber located at the Electric Propulsion Laboratory of the Phillips Laboratory at Edwards Air Force Base. The arcjet operates on a hydrogen gas flow of 13.1 mg/s (8.74 slpm) at an operating chamber pressure of 45 mtorr. The gas flow and power were chosen to closely match the conditions under which the most complete set of previous diagnostic data for a 1-kW hydrogen arcjet was taken, in order to facilitate comparisons between different data sets and between data and models.

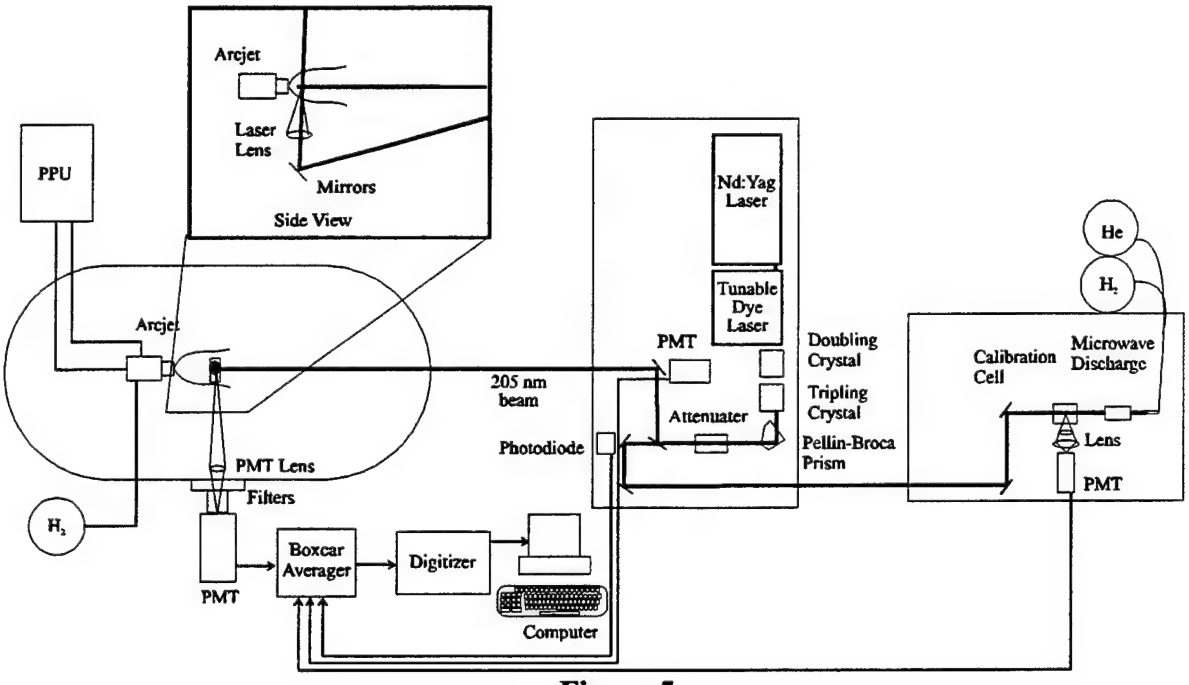

Figure 5
Experimental Setup for LIF Diagnostics

The laser is a pulsed dye laser pumped by a Nd:YAG with a repetition rate of 10 Hz and a pulse width of 6 ns. For the two-photon direct excitation method, the dye laser output was at 615 nm and was frequency-tripled to achieve about 0.5 mJ per pulse at 205 nm. A mirror turned about

80% of the beam toward the arcjet chamber through a variable attenuator placed in the beam; the remaining 20% of beam energy was directed toward a microwave-discharge source of atomic hydrogen.

For the single-laser two-step technique, the dye laser output was at 486 nm and was frequency doubled to achieve about 0.2 mJ per pulse at 243 nm; the lower energy was due to the weaker dye used in this wavelength range. The beams in the two-step technique needed to be brought together at the detection volume both spatially and temporally so a delay line in one beam could be required.

For axial velocity measurements, the beam was sent directly down the axis of the arcjet flow (Path 1) and was focused with a telescope lens configuration (not shown) outside the chamber with a focal length on the order of 2 m. For radial measurements, the unfocused beam was sent to a turning prism inside the chamber located underneath the arcjet (Path 2), directed to pass vertically through the plume, and was focused by a 200-mm-focal-length lens. The laser beam and optics remain fixed, while the arcjet was mounted on a motion control *xyz* stage to translate it for probing different regions of the plume.

A filtered PMT was placed behind the final turning mirror before the chamber in order to detect ASE that could propagate back along the laser beam path. A 200-mm-focal-length, 2-in-diameter lens was placed inside the chamber to collimate the LIF emitted toward the side window. The light was collected outside the chamber, focused through a 1-mm aperture, and detected with a filtered, gated PMT. Since the LIF occurs at 656 nm, the filters used were a 656-nm bandpass interference filter and an RG 645 color glass filter; scattered laser light (205 nm) was thus filtered out. The gated PMT is an ordinary Hamamatsu 928 tube with a special socket that was triggered to detect light for 2 μs during each laser pulse and was off between pulses. A gated integrator with a 30-ns gate was used to amplify and average the Hα fluorescence seen by the PMT. Alternatively, the PMT signal could be digitized by a fast oscilloscope to obtain fluorescence lifetimes and quenching information.

The weak UV beam that was sent into the discharge cell was focused with a 2-in-diameter, 150-mm-focal-length lens. The cell was run with a slow flow of a few torr of helium carrier gas and a few percent hydrogen through a microwave discharge tube. The LIF was detected through a filtered (ungated) PMT. Simultaneous detection of LIF from the cell during each spectral scan of the arcjet LIF provided a zero-velocity comparison from which Doppler shifts and room temperature Doppler widths could be measured. This discharge cell provided wavelength calibration but not density calibration. A separate discharge cell was used for density calibration and was placed inside the chamber when the arcjet is not operating.

The procedure for obtaining absolute number density is based on a method reported by Meier, *et al.*[24–27] After a relative number density scan and corresponding lifetime data are taken, the arcjet is then turned off and translated away from the collection volume, the chamber is opened, and a second calibration cell is placed in the detection volume with the laser beam passing through it. The LIF signal and lifetime are measured for the hydrogen atoms present in the cell. Atoms are present because of the flow of hydrogen through a microwave discharge prior to entering the cell.

Since the laser beam, detection optics and electronics have remained the same, the LIF from the arcjet and from the cell will have the same proportionality to absolute number density after correcting for any differences in quenching:

$$N_H^A = \frac{S^A}{S^C} \cdot N_H^C \cdot C_Q \tag{13}$$

Here S^A and S^C are the signal sizes (integrated over the entire spectral width) from the arcjet and the cell, N_H^A and N_H^C are the absolute number densities of atomic hydrogen in the arcjet and the cell, and C_Q is the scaling factor for the difference in quenching. C_Q is given by the ratio of fluorescence decay rate in the arcjet to that in the calibration cell.

The absolute number density of hydrogen atoms in the discharge cell is obtained using a standard chemical titration method. A schematic of the calibration cell used for this method is found in Figure 6. The cell is of glass tubing and is approximately 30 cm long and 5 cm in diameter. Important to the design of the cell is the long drift tube area with a polychloroethylene tubing liner to reduce gas/wall interactions. This drift tube allows complete mixing of the titration gas and the gas of interest. In this case, the titration gas is NO_2, and H is the gas to be calibrated.

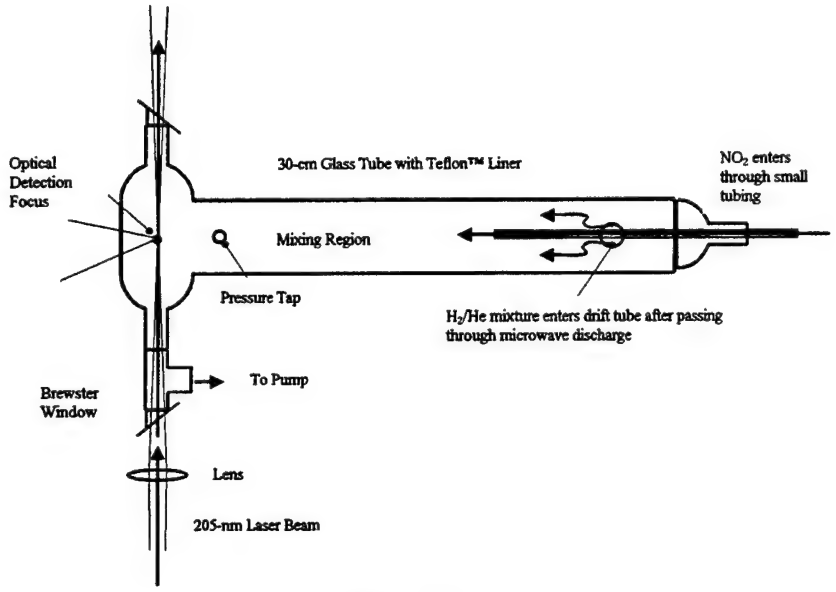

Figure 6
Calibration Cell Schematic

The hydrogen (with helium carrier gas) enters the drift tube area near one end after passing through a microwave discharge. A dilute mixture of NO_2 in helium is added to the flow through a long thin tube and enters the larger drift tube region at a location past the point where the hydrogen has entered. This reduces the amount of NO_2 that might diffuse upstream and enter the microwave discharge.

The NO_2 reacts rapidly with hydrogen atoms when the two are completely mixed in the large drift tube volume. The calibration involves flowing a 2% hydrogen in helium mixture and then the addition of 2% NO_2 in helium until the fluorescence signal decreases. A small vacuum pump brings the cell pressure to about 0.1 atm during this procedure.

The calibration involves observing the LIF signal decrease until it is gone at the point where the partial pressure of added NO_2 is equal to the partial pressure of hydrogen atoms in the cell. Control of the amount of NO_2 added allows the determination of the amount of hydrogen atoms present in the calibration cell. The NO_2 concentration at the point the fluorescence disappears is equal to the concentration of atomic hydrogen present as each hydrogen atom is reacted away for each NO_2 molecule added in the fast reaction

$$H + NO_2 \rightarrow OH + NO. \tag{14}$$

The large amount of buffer gas and low amount of H significantly reduce possible secondary reactions, making them negligible for the purposes of this experiment. Calibration takes place either before or after each arcjet firing.

Once a relative density profile has been taken, and quenching, ASE, MPI, and laser linewidth broadening have been compensated for or taken into account, an effective fluorescence measurement results, representing relative density in the arcjet plume. Through the method described in Section 2.1.2, a relationship between H atom density and a corrected effective LIF fluorescence for the calibration cell environment can be determined. If the correction factors in each environment are appropriately made to bring the fluorescence measured in each environment to a standard "ideal" condition equivalent, a relationship between the fluorescence measured in the arcjet plume and the corresponding atomic hydrogen number density can be made.

Figure 7 shows an axial scan involving simultaneous two-photon excitation of atomic hydrogen in a calibration cell and excitation of atomic hydrogen in a point 0.4 mm away from the nozzle exit in the arcjet plume. A Gaussian least-squares fit overlays the data and is used for determination of velocity, temperature, and density. In the figure, λ_0 and λ_1 are the wavelengths of the calibration profile and of the plume profile, respectively. Note that the fit for the cell is very good because the environment is quite static. The fit in the arcjet plume is not as good, though the fit width and center do appear to match the data quite well.

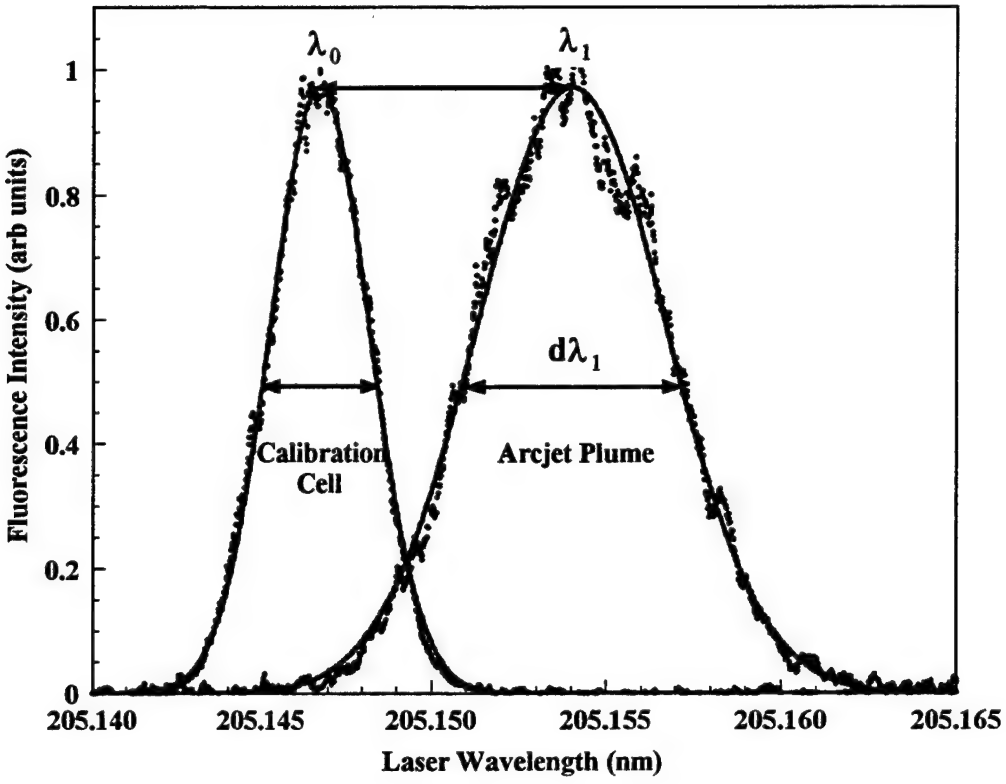

Figure 7
LIF Spectra of Calibration Cell and Arcjet Plume

The Doppler shift of the arcjet plume absorption line relative to the static absorption in the cell is evident, as is the Doppler width increase due to the much higher temperature in the arcjet plume relative to the room temperature in the calibration cell. The data correspond to a temperature near 2000 K and a velocity near 10 km/s. These numbers are rough since each of the broadening mechanisms were not fully accounted for in this analysis.

Figure 8 shows the fluorescence decay for n=3 hydrogen atoms at two positions along the arcjet nozzle exit plane. For comparison, a trace of the laser pulse alone (with no hydrogen atoms present) is shown.

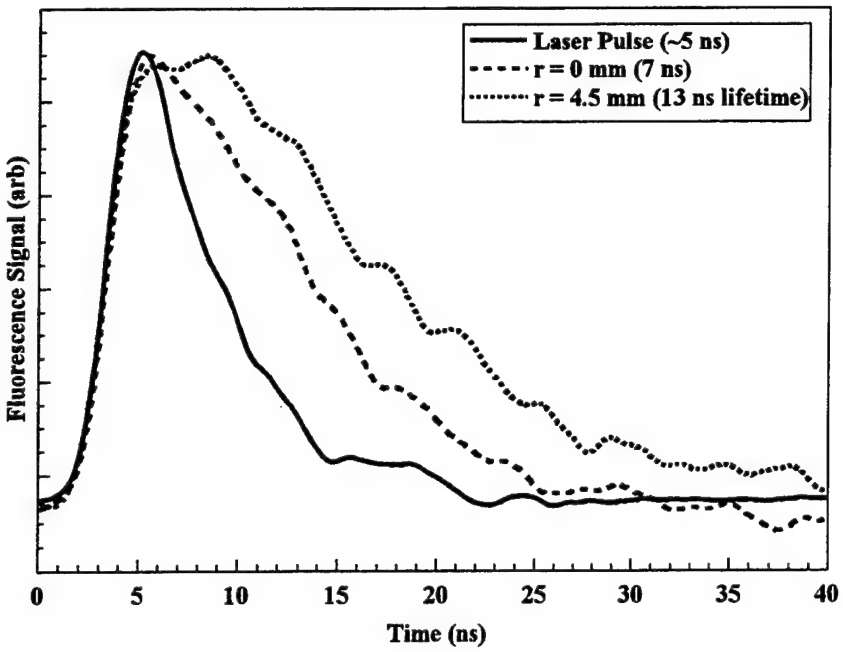

Figure 8
Fluorescence Decay at Two Radial Positions

To use the data in Figure 8 for a relative density measurement, the integrated area of the transition is compared with the integrated fluorescence area of data from another spatial location. To determine the correction for quenching at each spatial location, fluorescence lifetime measurements with a fast oscilloscope must be made. Figure 8 shows fluorescence measurements of the laser beam alone, the lifetime at the center of the plume and the lifetime near one edge near the nozzle exit. The lifetime of the unquenched transition is 15.7 ± 1.5 ns[28] so some collisional quenching is still evident even near the edge of the visible plume near the nozzle exit.

2.2 Current-Modulation Velocimetry

Although much research, both experimental and numerical, has been conducted on arcjet plumes over the last 30 years, almost all previous studies assumed that the arcjet operates in a steady-state mode. However, when current is provided by a high-frequency switching power supply, the current delivered to the arcjet is modulated at the power-processing unit (PPU) switching frequency. How current modulation affects overall arcjet thruster performance is not fully understood. Current modulation is thought to potentially play a role in electrode erosion effects, while Reference 39 clearly demonstrated that excited-state frozen-flow losses are affected by current modulation. It must still be resolved how current fluctuations affect mean velocity and frozen flow: dissociation, ionization, and vibrational and rotational energy losses. Furthermore, velocity fluctuations may lead to recoverable viscous losses.

To obtain velocity fluctuation data in an arcjet plume, it was necessary to develop a new velocity diagnostic. This diagnostic, called current-modulation velocimetry (CMV), measures

instantaneous velocity over a spatial region between two points. A current spike applied to the arcjet input current generates an optical event which is observed to travel downstream with the gas flow. Observing this event at two locations a fixed distance apart implies an average bulk velocity of the gas flowing out of the arcjet nozzle. CMV is the only technique that has been employed which provides instantaneous velocity measurements of the arcjet plasma with temporal resolution of a few microseconds. The disadvantages of CMV are that it employs spatial averaging over an axial distance of several millimeters and that it is a line-of-sight integrated technique.

In Reference 40, the CMV technique was used to measure fluctuations in velocity as large as ±20% of the mean velocity (Fig. 9). The source of the fluctuations in the gas velocity was not ascertained, though it was surmised that the velocity fluctuations might be linked to the ripple in the current applied to the arcjet.

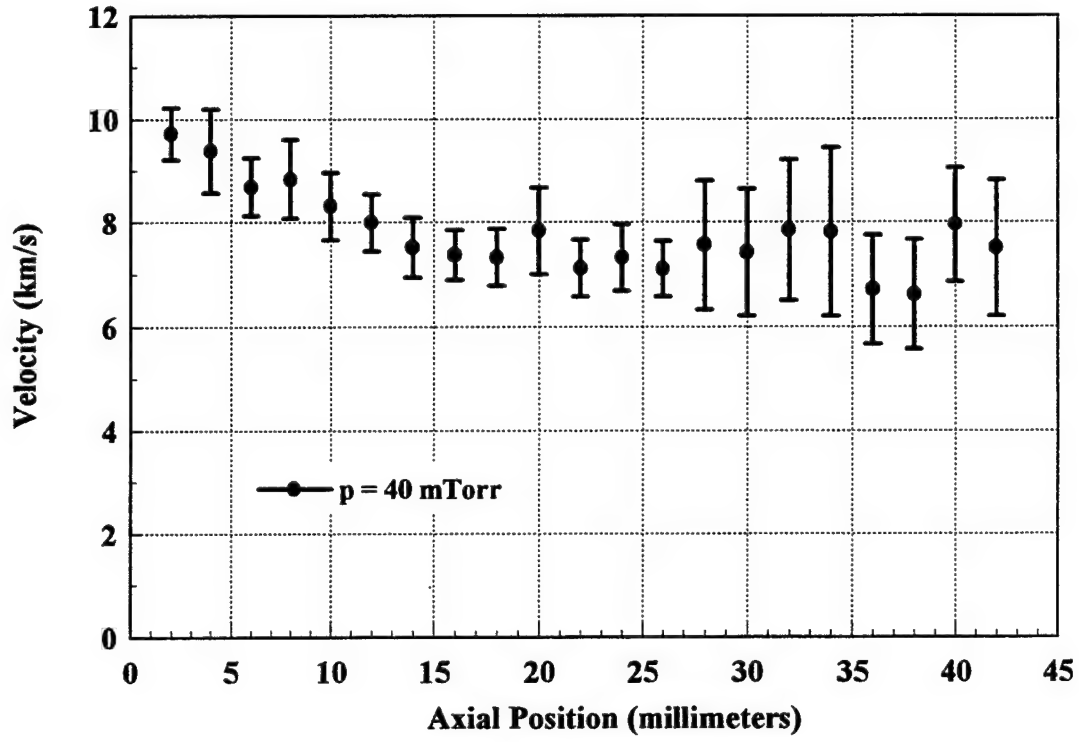

Figure 9
Mean Velocities and Fluctuations Downstream of Arcjet Nozzle Exit

The present work employs the use of an automated triggering circuit in conjunction with the CMV technique to measure velocity at a time when the current ripple is at a specified level. This allows multiple velocity measurements taken for statistical purposes to be triggered at the same phase in the current ripple.

CMV experiments were conducted in the Optical Diagnostics Chamber of the Air Force Phillips Laboratory's Electric Propulsion Laboratory. The arcjet used was a 1-kW-class radiatively cooled engine, constructed and furnished by NASA Lewis Research Center. Standard operating conditions were: 1.13 kW (112.5 V and 10.1 A), with 13.7 mg/s mass flow of hydrogen propellant. The experiments were conducted with a background chamber pressure of ~35 mtorr. The operating conditions are similar to those of other groups involved in optical diagnostic velocity measurements,[41] allowing comparison of experimental results to be made.

Power was provided by a NASA Lewis 1-kW PPU. The PPU is a high-frequency switching power supply, operating at 16 kHz, and generates a 20% peak-to-peak current ripple. The vacuum system consists of an aluminum chamber, 3 m in length and 2 m in diameter. Two 9500-cfm Roots blowers evacuate the chamber; each is backed by a 1600-cfm blower and a mechanical pump.

For the optical emission measurements, two Hamamatsu R943-02 PMTs were used. A 10-nm bandpass interference filter (Melles Griot; λ_0=656.3 nm) and appropriate neutral density filters were placed in front of each PMT to ensure that only the Hα emission was observed. The optics train of each detection system was identical. All optical, current and voltage signals were recorded on a Tektronix DSA 601 digital signal analyzer or a Tektronix TDS 644A digital oscilloscope.

The current spike needed for CMV is generated by a simple resistance-capacitance (RC) shunt circuit installed in parallel with the arcjet. Upon closing a switch between this circuit and the arcjet circuit, the arcjet voltage appears across the shunt, charging the capacitor over several 1-μs RC time constants. The shunt current is thus a several-ampere pulse lasting a few microseconds. The shunt current is subtracted from the arcjet current, which results in a spiked current dropout (the total current from the PPU is constant during this time, since it is held up by an output inductor of several millihenries).

The positive ring of the current pulse generates a sharp emission spike. A portion of the flow inside the arcjet is thus "tagged" by the current pulse. The emission spike is delayed with respect to the current spike; this delay is equal to the integral of $1/v$ over the distance from the arc-heating region to the detection station, where v is the plume velocity as a function of axial position.

The emission spike is recorded at two different downstream locations. A best-fit transformation between the two digitized emission spikes is determined using the standard Levenberg-Marquardt method.[34] The generated covariance matrix gives a measure of the confidence interval of the best-fit parameters, assuming the measurement of the optical signal to be subject to uniform, normally distributed scatter. Error bars indicate the precision of each measured velocity and are computed using a one-standard-deviation confidence interval of the horizontal translation (the time delay between the two emission spikes).

The current and emission spikes are a few microseconds long. The time delay between the emission spikes at the two locations can be resolved to within 1 ns, leading to a velocity

measurement whose accuracy is in the range of 30 to 60 m/s for plume velocities on the order of 5 to 0 km/s; this accuracy is comparable to those of recent LIF results.[3,41,42]

Note that the velocity measurements obtained with CMV, while still position-averaged over the detector separation (here, 3.29±0.05 mm), are instantaneous. The principal velocity diagnostics presently being used for arcjets are continuous-wave[41,42] and pulsed[43] LIF, which provide spatially resolved mean velocity measurements but with very limited temporal resolution. LIF measurements determine the absorption lineshape by scanning in laser wavelength, which takes a minimum of several seconds to determine a velocity. In principle, a Doppler-shifted emission lineshape could be recorded instantaneously by a spectrograph and a gated imaging detector, but it is not known if there are any plume measurements in which Doppler shifts have been so measured. (In the recent Stuttgart work of Zube and Auweter-Kurtz,[43] instantaneous lineshapes were recorded in order to measure gas excitation temperature and electron density in the arc.)

An automatic opto-isolated switch circuit allowed computer control of the start time and duration of the modulation to the arcjet current (Fig. 10). The switch closure is triggered by a pulse generator. The generator issues a pulse when the measured arcjet current reaches a preset level and after a computer request for an event has been received. This allows the operator to issue a request for a measurement and have that measurement take place the next time the PPU current ripple is at the specified phase.

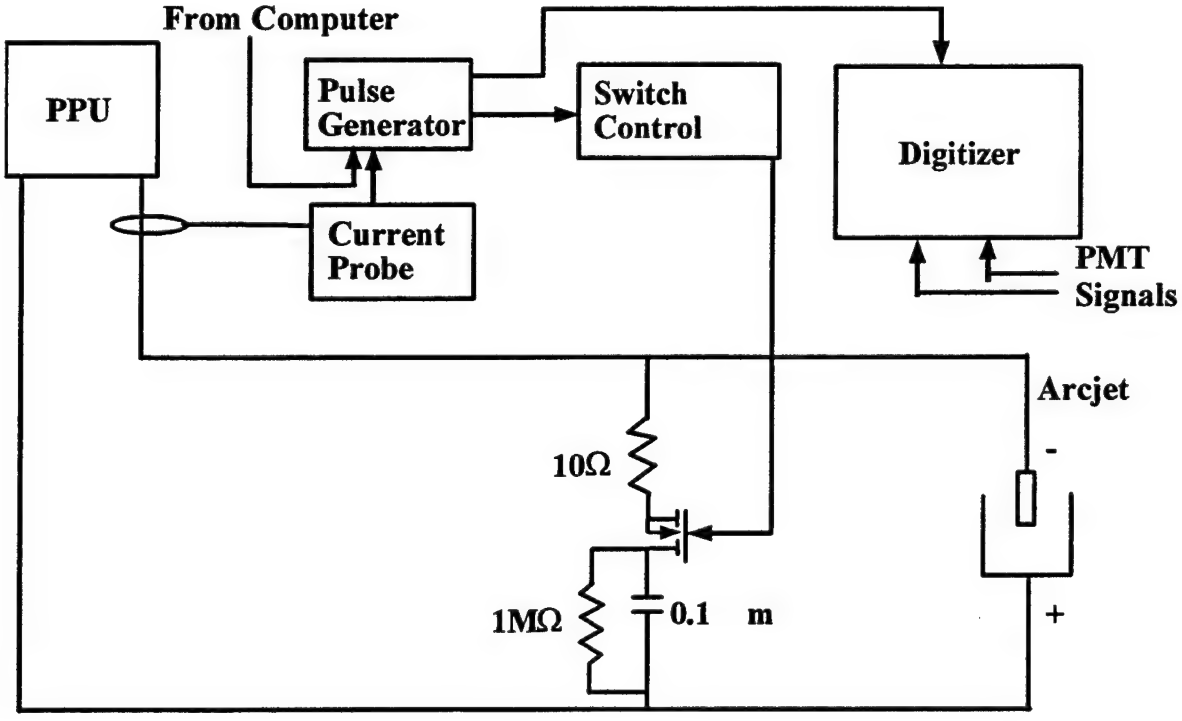

Figure 10
Automated CMV Setup

Figure 11 illustrates the effect of the CMV technique on the arcjet's current and voltage. The PPU-induced arcjet current ripple is briefly interrupted while the capacitor charges. The current then rings upward and significantly overshoots its previous maximum. After quickly dampening, the current begins its previous PPU-induced ripple. Note that the voltage across the arcjet also has a characteristic ripple and that it is almost 180° out of phase of the current. This is an expected consequence of the negative impedance characteristic of arcjet devices.[40]

Figure 11 reveals an unexpected behavior of the arcjet voltage that occurs as current is redirected into the capacitor of the RC circuit. The voltage drops suddenly as the current drops and then gradually ramps upward to previous levels without ringing. It then begins its periodic ripple.

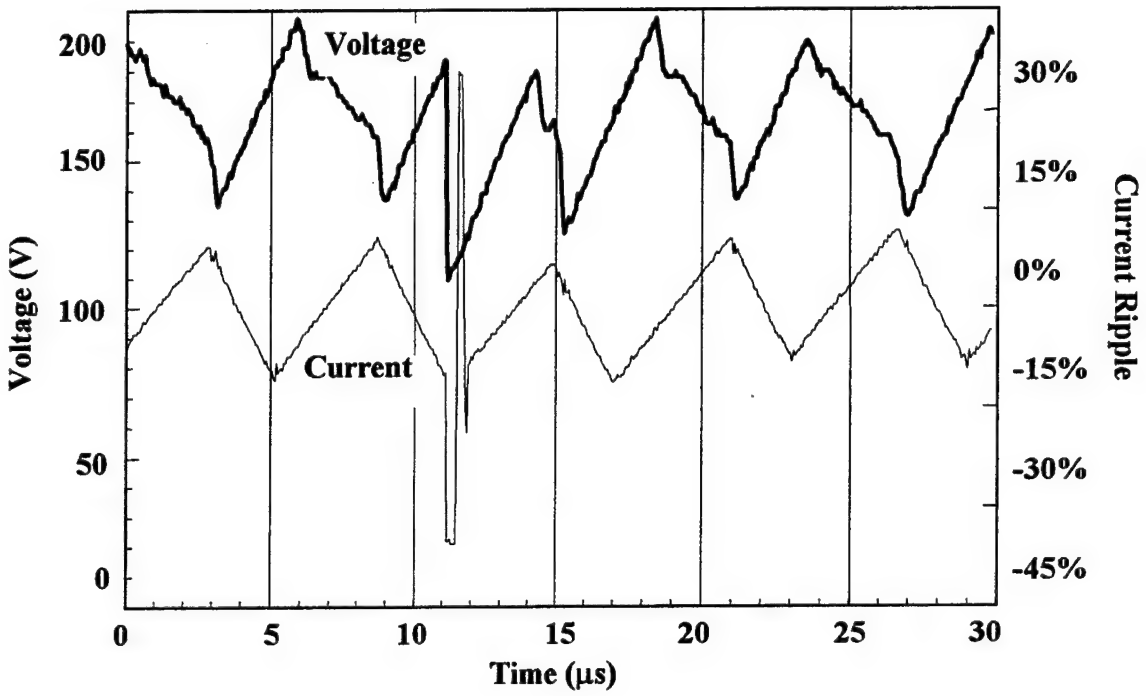

Figure 11
Typical CMV Effect on Arcjet Current and Voltage

Figure 12 gives the current and voltage on a shorter timescale. The voltage and current both drop quickly after the CMV gate pulse closes the circuit and then simultaneously change in slope. The voltage begins to ramp back upward to previous levels, while the current decreases in a more gradual way then before. At time 11.5 μs, the current then shoots upward with no apparent reaction by the arcjet voltage. It then returns to previous levels with some minimal ringing.

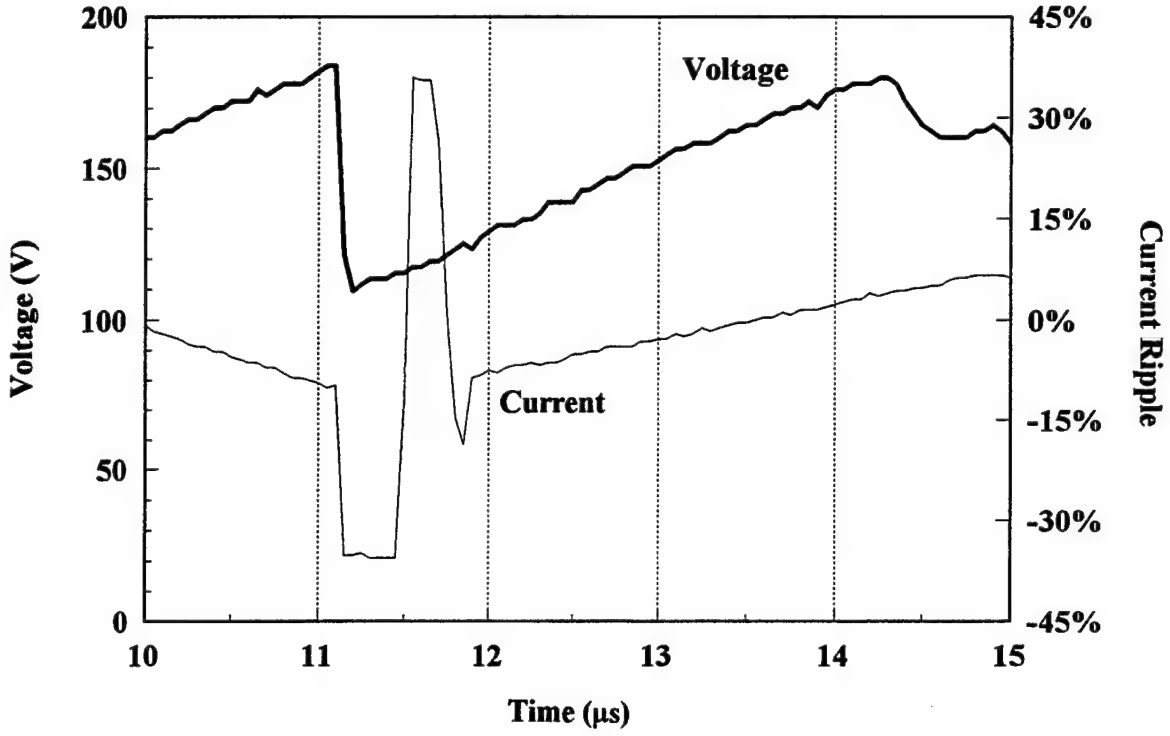

Figure 12
Typical CMV Effect on Arcjet Current and Voltage, Shorter Time Scale

In addition to arcjet current and voltage probes, a Hall-effect current probe was placed on the RC circuit. Two digitizing oscilloscopes were used in order to simultaneously observe several transient signals. These include the arcjet current and voltage, the current through the circuit when the switch is closed, the gate controlling the switch, and the two emission traces taken from the PMTs. The resulting scope traces are shown together in Figure 13.

The current measured through the circuit is complementary to the current going to the arcjet, as expected. When the circuit current drops below its initial level (no current through the circuit), it indicates that current through the circuit has reversed direction and that the capacitor is discharging; this is an expected reason for the arcjet current to overshoot. The arcjet current rapidly decreases, dropping below its initial level, and a short ring in circuit current is seen. This is followed by a slow rise back up to zero in circuit current and a return to previous ripple behavior in arc current.

As noted earlier in this section, the arcjet voltage follows the current when the CMV gate is closed and decreases in value rapidly. As current begins to flow through the circuit, however, the arcjet voltage begins a slow rise back to its previous level, seemingly unaffected by other changes in arcjet current.

All optical events are observed downstream of the arcjet nozzle exit plane. One PMT (with a hydrogen Hα notch filter) is focused to a small control volume of diameter 1 mm from the nozzle exit centerline, while a second identical PMT system is focused to a control volume located 3.29 mm downstream of the nozzle exit. Noise in the optical emission, which starts at 4 μs in Figure 13, is seen simultaneously by both PMTs when the arcjet current first begins to rise. This is then followed by a much more significant increase in Hα emission at 6 μs. This increase occurs at both control volumes but at different times; it is seen first at the upstream PMT focal point.

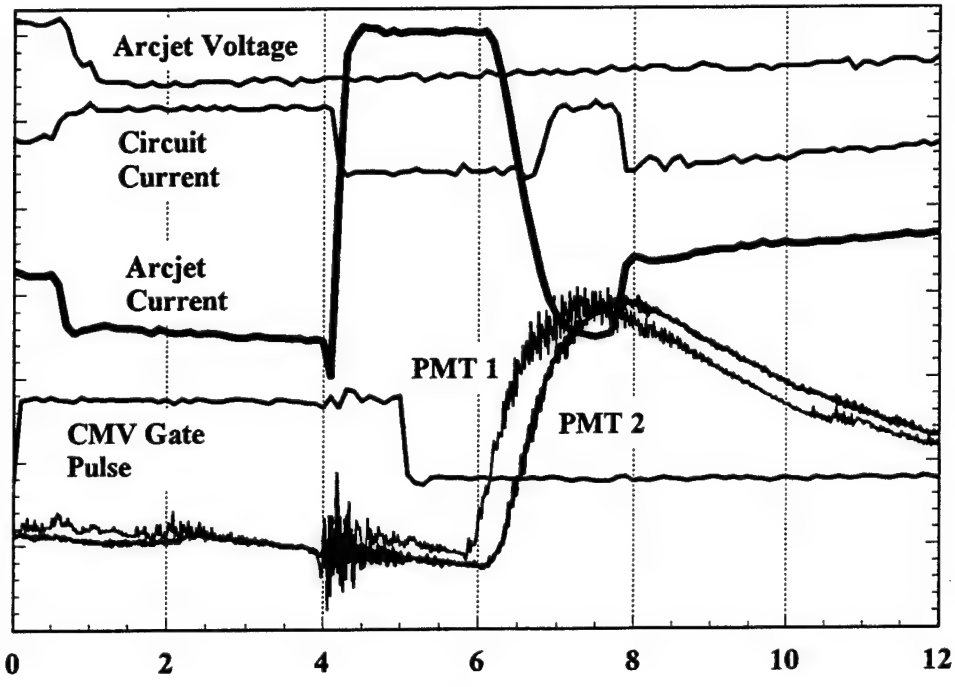

Figure 13
Arcjet and CMV Properties versus Time, Arbitrary Units on Ordinate

The optical noise seen as the arcjet current first rises does not demonstrate a time shift as does the emission that follows it. Thus, the two different emission phenomena seen at 4 and 6 μs are most likely caused by different excitation processes.

In Reference 40, it was stated that the optical emission phenomenon that progresses downstream in the plume comes from electron recombination which repopulates the uppermost energy levels of the H atom. The electrons subsequently cascade downward to repopulate the n=*3* excited state, which is then observed by the PMTs as Hα emission. This explanation still appears valid for the large time-dependent emission peaks that begin at 6 μs. However, the optical noise seen at 4 μs must warrant a separate explanation because of its time-independent nature. It is likely that the optical emission at 4 μs in the arcjet plume is caused by the reabsorption of photons

generated at the arc core inside the constrictor region of the arcjet, as suggested by Crofton, *et al.*[44]

When starting the arcjet, the voltage characteristic of the thruster changes slowly as the nozzle heats up. The mean voltage increases while the heating takes place. Prior to reaching a steady-state voltage a curious behavior is noted to intermittently take place when implementing the CMV technique. Though the proper trigger gate and initial current behavior remain the same, differences in the current overshoot appear to lead to a situation where the emission spikes used for velocimetry do not appear. This situation is shown in Figure 14.

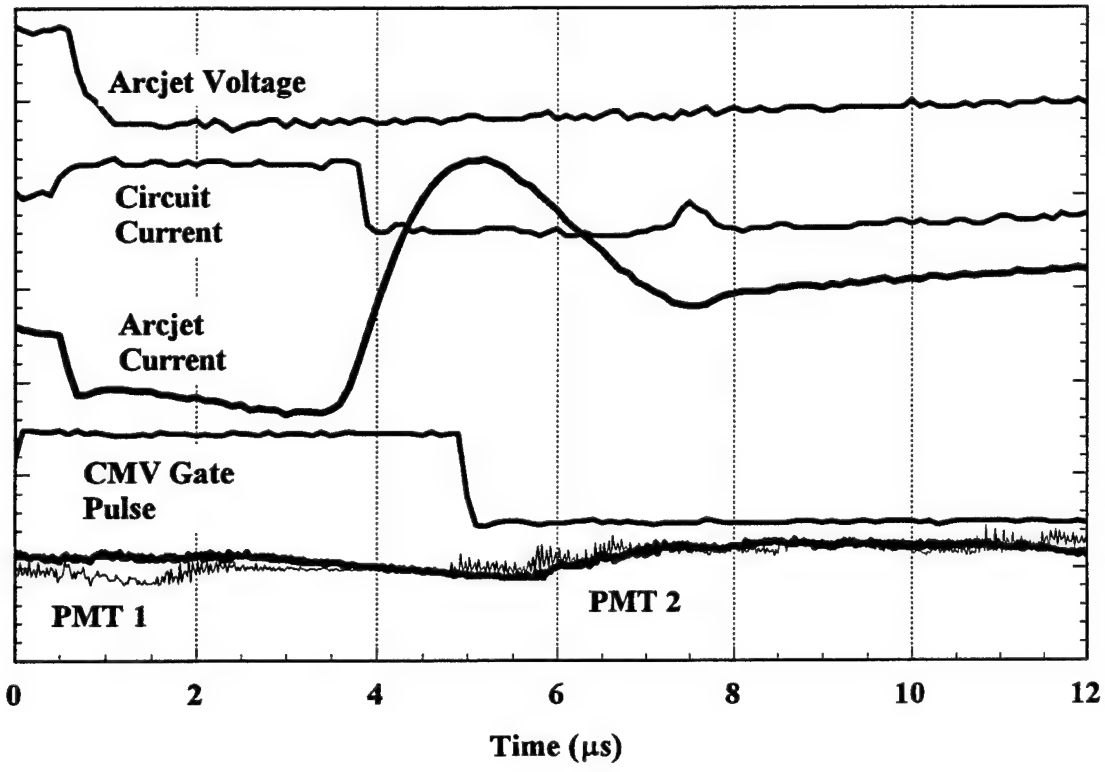

Figure 14
Arcjet and CMV Properties versus Time, No CMV Emission

Note that the first 4 μs of the "non-emission" case are essentially identical to the previous case depicted in Figure 13 where Hα emission is present. The sharp rise in current that followed in Figure 13 is not present, and both types of emission previously observed are absent. This prevents a CMV velocity measurement from being made and appears only in situations where the arcjet voltage is lower than the standard operating condition of 112.5 V and 10.1 A. As the arcjet is operated at lower current (and consequently higher voltage) this behavior is no longer seen. Therefore, the implementation of the CMV technique appears to rely on a minimum voltage across the arcjet in order to generate a subsequent ringing in the arcjet current when current is redirected into an RC circuit. It is likely that this subsequent ringing is the key phenomenon,

inducing the emission which proceeds downstream, thus allowing time-of-flight velocity measurements to be made.

To make velocity measurements while linked to the PPU current ripple, a computer-controlled switch was implemented. In using this switch a new parameter in CMV operation was required, the length of time that the RC circuit was closed (the gate width) in parallel with the arcjet. Results from varying the gate width are shown in Figure 15.

The gate width was varied from 0.5 ms to hundreds of milliseconds in length. The mean velocity measured was basically the same as long as the gate width was above 3 ms. Mean velocities measured were observed to decrease as the pulse width was decreased for the equivalent test conditions. Figure 15 demonstrates this behavior for three different power conditions. The $\frac{P}{\dot{m}}$ was held constant by reducing the mass flow through the arcjet as power was decreased. Note that for the 1.13 kW case, the decrease in velocity measured was less evident than in the lower power cases.

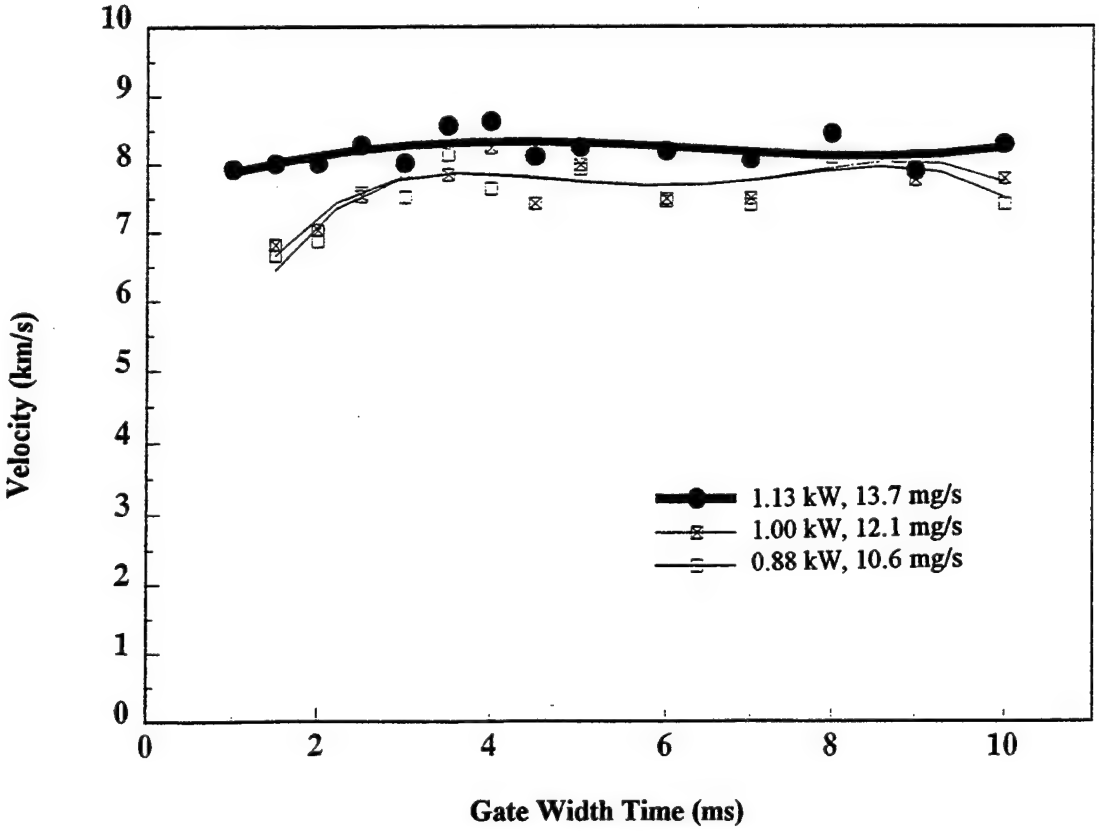

Figure 15
Measured Velocity versus Gate Width for Several Arcjet Power Levels

The shorter gate widths cause a change in measured velocity between the two emission collection points in the plume. When the RC circuit is connected to the arcjet for less than 3 μs, the behavior of current and voltage is similar to that seen in Figure 7 where the voltage is insufficient for CMV emission to take place. The short-gate-width behavior differs from that of Figure 13 since CMV emission occurs, though at lower intensities than desirable.

These lower velocity measurements are not due to a lower signal intensity but are suspect in the fact that the emission shape is less defined. It is possible that the recombination processes that repopulate the uppermost electronic levels are incomplete when the circuit is in parallel with the arcjet for short durations. It is surmised that the lower velocities result from utilizing a waveform that undergoes change as it traverses between the two imaging control volumes.

The average velocity measured at the nozzle exit, as well as the standard deviation of velocity fluctuations using CMV with a gate width larger than 3 μs, is shown in Figure 16 along with LIF longitudinal velocity data from Liebeskind, *et al.*[41]

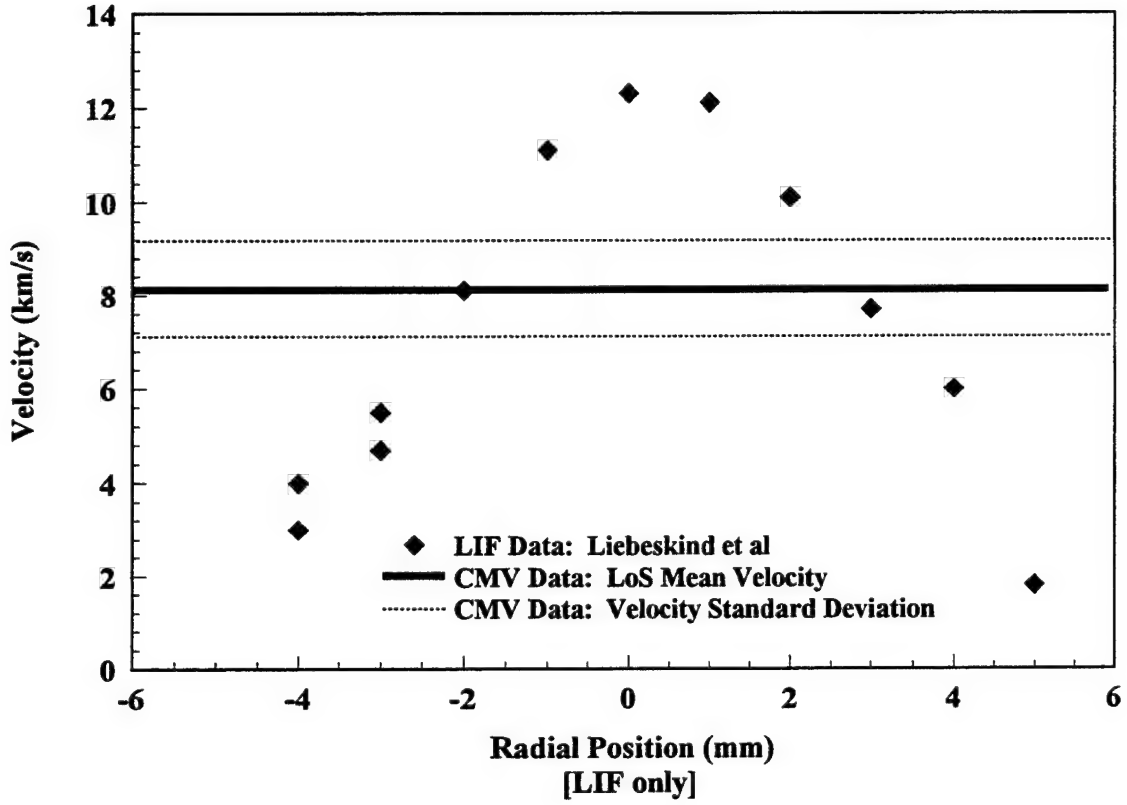

Figure 16
CMV and LIF[41] 1-kW Arcjet Velocities at Nozzle Exit

In this figure, radial, point-specific, time-averaged LIF velocity measurements are compared with a line-of-sight-averaged CMV velocity shown as a line across the graph, with two dashed lines representing the standard deviation of observed velocity fluctuations. Though the density of excited-state H is not available to weigh the LIF data and obtain a mean LIF velocity, relatively good agreement between these two techniques is observed.

It has previously been surmised that the fluctuations in Figure 9 and in Reference 40 were a consequence of the oscillating nature of the internal energy dissipation of a 1-kW arcjet caused by the PPU current modulations. Triggering at a constant PPU ripple level, Figure 17 shows measured mean velocity and standard deviations while triggering at constant current ripple phase.

In Figure 17, no change in mean velocity value or substantive change in fluctuations can be directly related to PPU phase angle. If the velocity is changing with respect to the current ripple, a significant decrease in fluctuation and change in mean velocity should be observed.

With no apparent connection between the PPU ripple and the mean velocity, the question arises once again: What is causing the fluctuations in arcjet plume velocity? Attempts to determine a fluctuation frequency through a real-time transformation of the difference between the emission from the two imaging points provided inconclusive results. Certainly finding a fundamental frequency of velocity fluctuation might narrow the possible causes of this phenomenon, though it remains to be seen if a single cause can be pinpointed.

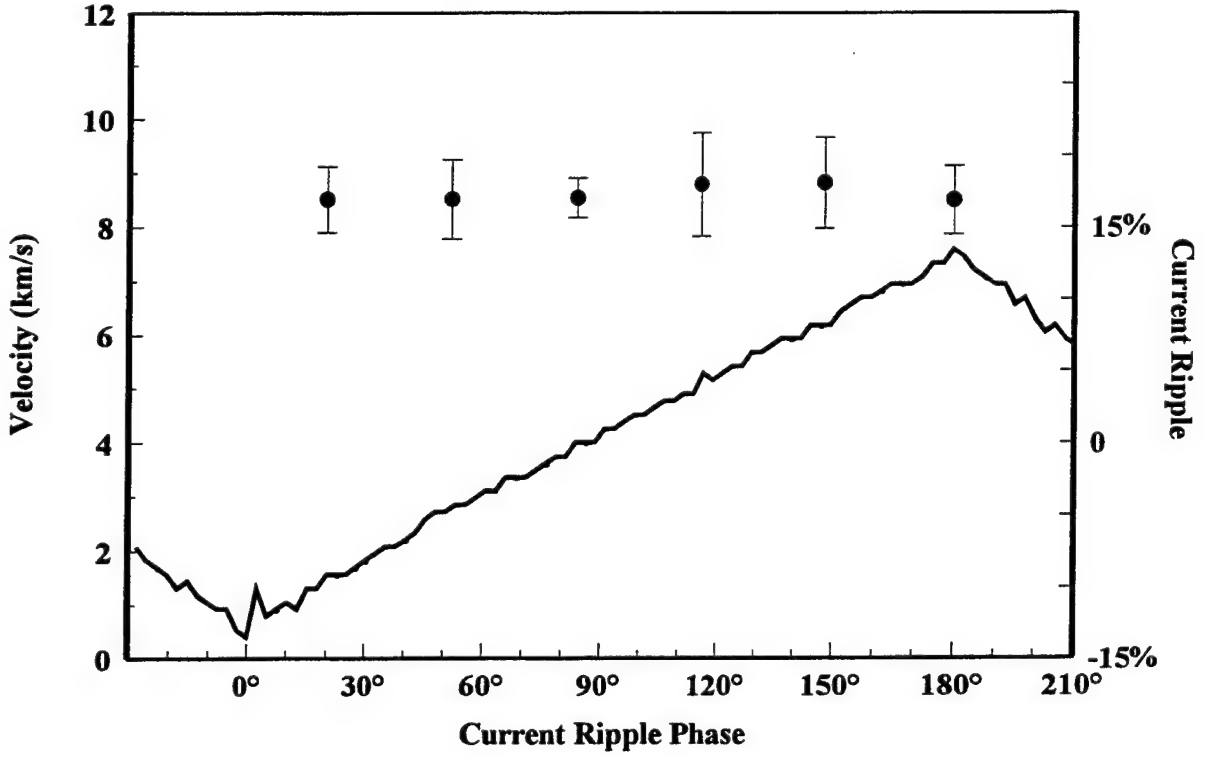

Figure 17
CMV Exit Plane Velocity Measurements at Various Current Ripple Phases

3.0 CONCLUSIONS

In this work, several innovative approaches to experimental diagnostics of arcjet operation were developed. For the first time, measurements of ground-state atomic hydrogen were made in a powered-up arcjet. These measurements are in accord with published computational results to within the experimental accuracy. The measurements need to be extended to produce a comprehensive density map of the plume; this part of the work was expected to be completed during the period of the contract, but both density-measurement techniques (pulsed electron-beam fluorescence and two-photon laser-induced fluorescence) experienced unexpected protraction during development and are only now reaching sufficient maturity.

The other technique used in this work, current-modulation velocimetry, was applied to the problem of measuring the time dependence of arcjet plume velocity fluctuations. These fluctuations bore no measurable correlation with supply current ripple and appeared to be random. The impact of this conclusion on time-dependent arcjet modeling is not yet obvious.

REFERENCES

1. Smith, W.W., *et al.*, "Low Power Hydrazine Arcjet System Flight Qualification," IEPC-91-148, presented at the AIDAA/AIAA/DGLR/JSASS 22nd International Electric Propulsion Conference, Viareggio, Italy, 14-17 Oct, 1991.

2. Vaughan, C.E., and Cassady, R.J., "An Updated Assessment of Electric Propulsion Technology for Near-Earth Space Missions," AIAA-92-3202, presented at the 28th AIAA/SAE/ASME/ASEE Joint Propulsion Conference, Nashville, TN, 6-8 Jul, 1992.

3. Erwin, D.A., Pham-Van-Diep, G.C., and Deininger, W.D., "Laser-Induced Fluorescence Measurements of Flow Velocity in High-Power Arcjet Thruster Plumes," *AIAA Journal*, **29,** Aug 1991, pp. 1298-303.

4. Liebeskind, J.G., Hanson, R.K., and Cappelli, M.A., "Laser-Induced Fluorescence Diagnostic for Temperature and Velocity Measurements in a Hydrogen Arcjet Plume," *Appl. Opt.*, **32**, *30*, 20 Oct 1993, pp. 6117-27.

5. Manzella, D.H. and Cappelli, M.A., Vacuum Ultraviolet Absorption in a Hydrogen Arcjet," AIAA-92-3564, presented at the 28th AIAA/SAE/ASME/ASEE Joint Propulsion Conference, Nashville, TN, 6-8 Jul, 1992.

6. Pollard, J.E., "Arcjet Diagnostics by XUV Absorption Spectroscopy," AIAA-92-2966, presented at the 23rd AIAA Plasmadynamics and Lasers Conference, Nashville, TN, 6-8 Jul, 1992.

7. Keefer, D., Burtner, D., Moeller, T., and Rhodes, R., "Multiplexed Laser Induced Fluorescence and Non-Equilibrium Processes in Arcjets," AIAA-94-2656, presented at the 25th AIAA Plasmadynamics and Lasers Conference, Colorado Springs, CO, 20-23 Jun, 1994.

8. Butler, G.W., Boyd, I.D., and Cappelli, M.A., "Non-Equilibrium Flow Phenomena in Low Power Hydrogen Arcjets," AIAA-95-2819, presented at the 31st AIAA/ASME/SAE/ASEE Joint Propulsion Conference, San Diego, CA, 10-12 Jul, 1995.

9. Babu, V., Aithal, S.M., and Subramaniam, V.V., "Propellant Internal Mode Dis-Equilibrium and Frozen Flow Losses in Arcjets," AIAA-94-2655, presented at the 25th AIAA Plasmadynamics and Lasers Conference, Colorado Springs, CO, 20-23 Jun, 1994.

10. Miller, S., and Martinez-Sanchez, M., "Nonequilibrium Numerical Simulation of Radiation-Cooled Arcjet Thrusters," IEPC-93-218, presented at the 23rd International Electric Propulsion Conference, Seattle, WA, Sep 1993.

11. Megli, T.W., Krier, H., and Burton, R.L., "A Plasmadynamics Model for Nonequilibrium Process in N_2/H_2 Arcjets," AIAA-95-1961, presented at the 26th AIAA Plasmadynamics and Lasers Conference, San Diego, CA, 19-22 Jun 1995.

12. Boyd, I.D., Cappelli, M.A., and Beattie, D.R., "Monte Carlo and Experimental Studies of Nozzle Flow in a Low-Power Hydrogen Arcjet," AIAA-93-2529, presented at the 29th AIAA/SAW/ASME/ASEE Joint Propulsion Conference, Monterey, CA, 28-30 Jun, 1993.

13. Beattie, D.R., and Cappelli, M.A., "Molecular Hydrogen Raman Scattering in a Low Power Arcjet Thruster," AIAA-92-3566, presented at the 28th AIAA/SAE/ASME/ASEE Joint Propulsion Conference, Nashville, TN, 6-8 Jul, 1992.

14. Beattie, D.R., and Cappelli, M.A., "Raman Scattering Measurements of Molecular Hydrogen in an Arcjet Thruster Plume," AIAA-95-1956, presented at the 26th AIAA Plasmadynamics and Lasers Conference, San Diego, CA, 19-22 Jun, 1995.

15. Goldsmith, J.E.M., Miller, J. A., Anderson, R. J. M., and Williams, L. R., "Multiphoton Excited Fluorescence Measurements of Absolute Concentration Profiles of Atomic Hydrogen in Low-Pressure Flames," **Twenty-Third Symposium (International) on Combustion**, The Combustion Institute, Pittsburgh, PA, 1990, pp. 1821.

16. Goldsmith, J.E.M. and Rahn, L.A., "Doppler-Free Two-Photon-Excited Fluorescence Spectroscopy of Atomic Hydrogen in Flames," *Opt. Lett.*, **15**, *14*, 15 Jul 1990, pp. 814-16.

17. Goldsmith, J.E.M. and Laurendeau, N.M., "Single-Laser Two-Step Fluorescence Detection of Atomic Hydrogen in Flames," *Opt. Lett.*, **15**, *10*, 15 May 1990, pp. 576-8.

18. Goldsmith, J.E.M., "Investigation of Simultaneous Two-Photon H and Single Photon OH Excitation in Flames Using a Single Dye Laser," *Appl. Opt.*, **29**, 20 Nov 1990, pp. 4841-2.

19. Goldsmith, J.E.M., Anderson, R.J.M., and Williams, L.R., "Time-Resolved Two-Photon-Excited Fluorescence Detection of Atomic Hydrogen in Flames," *Opt. Lett.*, **15**, *1*, 1 Jan 1990, pp. 78-80.

20. Westblom, U., Agrup, S., Alden, M., Hertz, H.M., and Goldsmith, J.E.M., "Properties of Laser-Induced Stimulated Emission for Diagnostic Purposes," *Appl. Phys.* B, **B50**, *6*, Jun 1990, pp. 487-98.

21. Goldsmith, J.E.M., "Two-Photon-Excited Stimulated Emission from Atomic Hydrogen in Flames," *J. Opt. Soc. Am. B, (Opt. Phys).*, **6**, Nov 1989, pp. 1979-85.

22. Goldsmith, J.E.M., "Multiphoton Excited Fluorescence Measurements of Atomic Hydrogen in Low-Pressure Flames," **Twenty-Second Symposium (International) on Combustion, The Combustion Institute**, Pittsburgh, PA, 1988, pp. 1403.

23. Goldsmith, J.E.M., "Two-Step Saturated Fluorescence Detection of Atomic Hydrogen in Flames," *Opt. Lett.*, **10**, *3*, Mar 1985, pp. 116-18.

24. Meier, U., Kohse-Hoinghaus, K., Schaefer, L., and Klages, C.-P., "Two-Photon Excited LIF Determination of H-Atom Concentrations Near a Heated Filament in a Low Pressure H_2 Environment," *Appl. Opt.*, **29**, *33*, 20 Nov 1990, pp. 4993-9.

25. Bittner, J., Kohse-Hoinghaus, K., Meier, U., Kelm, S., and Just, T.H., "Determination of absolute H Atom Concentrations in Low-Pressure Flames by Two-Photon Laser-Excited Fluorescence," *Combustion and Flame*, **71**, *1*, Jan 1988, pp. 41-50.

26. Meier, U., Bittner, J., Kohse-Hoinghaus, K., and Just, T. H., "Discussion of Two-Photon Laser-Excited Fluorescence as a Method for Quantitative Detection of Oxygen Atoms in Flames," **Twenty-Second Symposium (International) on Combustion, The Combustion Institute**, Pittsburgh, PA, 1988, pp. 1887.

27. Meier, U., Kohse-Hoinghaus, K., and Just, T.H., "H and O Atom Detection for Combustion Applications: Study of Quenching and Laser Photolysis Effects," *Chem. Phys. Lett.*, **126**, *6*, 23 May 1986, pp. 567-73.

28. Tserepi, A.D., Dunlop, J.R., Preppernau, B.L., and Miller, T.A., "Absolute H-Atom Concentration Profiles in Continuous and Pulsed RF Discharges," *J. Appl. Phys.*, **72**, *7*, 1 Oct 1992, pp. 2638-43.

29. Preppernau, B.L., Dolson, D.A., Gottscho, R.A., and Miller, T.A., "Temporally Resolved Laser Diagnostic Measurements of Atomic Hydrogen Concentrations in RF Plasma Discharges," *Plasma Chem. and Plasma Proc.*, **9**, *2*, Jun 1989, pp. 157-64.

30. Czarnetski, U., Miyazaki, K., Kajiwara, T., Muraoka, K., Maeda, M. and Dobele, H.F., "Comparison of Various Two-Photon Excitation Schemes for Laser-Induced Fluorescence Spectroscopy in Atomic Hydrogen," *J. Opt. Soc. Am. B (Opt. Phys.)*, **11**, *11*, Nov 1994, pp. 2155-62.

31. Muraoka, K., and Maeda, M., "Application of Laser-Induced Fluorescence to High-Temperature Plasmas," *Plasma Phys. and Controlled Fusion*, **35**, *6*, Jun 1993, pp. 633-56.

32. Eckbreth, A.C., **Laser Diagnostics for Combustion Temperature and Species, 1st ed.** Kent: Abacus, 1988.

33. Demtröder, W., **Laser Spectroscopy: Basic Concepts and Instrumentation,** Berlin: Springer-Verlag, 1988.

34. Press, W.H., Flannery, B.P., Teukolsky, S.A., and Vetterling, W.T., **Numerical Recipes: The Art of Scientific Computing, 1st ed.** Cambridge: Cambridge, 1986.

35. Bamford, D.J., Jusinski, L.E., and Bischel, W.K., "Absolute Two-Photon Absorption and Three-Photon Ionization Cross Sections for Atomic Oxygen," *Phys. Rev. A*, **34**, *1*, Jul 1986, pp. 185-98.

36. Georgiev, N., Nyholm, K., Fritzon, R., and Alden, M., "Developments of the Amplified Stimulated Emission Technique for Spatially Resolved Species Detection in Flames," *Opt. Comm.*, **108**, *1-3*, 15 May 1994, pp. 71-6.

37. Brown, M.S., and Jeffries, J.B., "Measurement of Atomic Concentrations in Reacting Flows Through the Use of Stimulated Gain or Loss," *Appl. Opt.*, **34**, *6*, 20 Feb 1995, pp. 1127-32.

38. Storm, P.V., and Cappelli, M.A., "High Spectral Resolution Emission Study of a Low Power Hydrogen Arcjet Plume," AIAA-95-1960, presented at the 26th AIAA Plasmadynamics and Lasers Conference, San Diego, CA, 19-22 Jun, 1995.

39. Spores, R.A., Pobst, J.A., Schilling, J.H., and Erwin, D.A., "Performance Effects of Interaction Between a Low-Power Arcjet and its Power Processing Unit," AIAA-92-3238, presented at the 28th AIAA/SAE/ASME/ASEE Joint Propulsion Conference, 6-8 Jul, 1992.

40. Pobst, J.A., Schilling, J.H., Erwin, D.A., and Spores, R.A., "Time Resolved Measurements of 1 kW Arcjet Plumes using Current Modulation Velocimetry and Triple Langmuir Probes," IEPC-93-128, , presented at the 23rd International Electric Propulsion Conference, Seattle, WA, Sep 1993.

41. Liebeskind, J.G., Hanson, R.K., and Cappelli, M.A., "Plume Characteristics of an Arcjet Thruster," AIAA-93-2530, presented at the 29th AIAA/SAE/ASME/ASEE Joint Propulsion Conference, Monterey, CA, 28-30 Jun, 1993.

42. Keefer, D., *et al.*, "Laser Fluorescence Velocimetry of Arcjet Exhaust Plume," IEPC-91-093, presented at the AIDAA/AIAA/DGLR/JSASS 22nd International Electric Propulsion Conference, Viareggio, Italy, 14-17 Oct, 1991.

43. Zube, D.M., and Auweter-Kurtz, M., "Spectroscopic Arcjet Diagnostic Under Thermal Equilibrium and Nonequilibrium Conditions," AIAA-93-1792, presented at the 29th AIAA/SAE/ASME/ASEE Joint Propulsion Conference, Monterey, CA, 28-30 Jun, 1993.

44. Crofton, M.W., Welle, R.P., Janson, S.W., and Cohen, R.B., "Rotational and Vibrational Temperatures in the Plume of a 1 kW Arcjet," AIAA-91-1491, presented at the 22nd AIAA Fluid Dynamics, Plasma Dynamics and Lasers Conference, Honolulu, HI, 24-26 Jun 1991.

45. Cappelli, M. A., Liebeskind, J. G., Hanson, R. K., Butler, G. W., and King, D. Q., "A Direct Comparison of Hydrogen Arcjet Thruster Properties to Model Predictions, " IEPC-93-220, presented at the 23rd International Electric Propulsion Conference, Seattle, WA, Sep 1993.